polymers

MDPI

Article

Enhanced Photovoltaic Performance in D-π-A Copolymers Containing Triisopropylsilylethynyl-Substituted Dithienobenzodithiophene by Modulating the Electron-Deficient Units

Junfeng Tong [1,*], Lili An [2], Jie Lv [1], Pengzhi Guo [3], Xunchang Wang [4], Chunyan Yang [1] and Yangjun Xia [1,*]

1 School of Materials Science and Engineering, Lanzhou Jiaotong University, Lanzhou 730070, China; zoeyejie@163.com (J.L.); YChY-5@126.com (C.Y.)
2 School of Chemical Engineering, Northwest Minzu University, Lanzhou 730030, China; anlili2011@163.com
3 National Green Coating Technology and Equipment Research Center, Lanzhou Jiaotong University, Lanzhou 730070, China; shxygpz@126.com
4 CAS Key Laboratory of Bio-Based Materials, Qingdao Institute of Bioenergy and Bioprocess Technology, Chinese Academy of Sciences, Qingdao 266101, China; wang_xc@qibebt.ac.cn
* Correspondence: tongjunfeng139@163.com (J.T.); xiayangjun2015@126.com (Y.X.); Tel.: +86-931-495-6022 (J.T. & Y.X.)

Received: 23 November 2018; Accepted: 19 December 2018; Published: 21 December 2018

Abstract: Three alternated D-π-A type 5,10-bis(triisopropylsilylethynyl)dithieno[2,3-*d*:2′,3′-*d*′]-benzo[1,2-*b*:4,5-*b*′]dithiophene (DTBDT-TIPS)-based semiconducting conjugated copolymers (CPs), PDTBDT-TIPS-DTBT-OD, PDTBDT-TIPS-DTFBT-OD, and PDTBDT-TIPS-DTNT-OD, bearing different A units, including benzothiadiazole (BT), 5,6-difluorinated-BT (FBT) and naphtho[1,2-*c*:5,6-*c*′]-bis[1,2,5]thiadiazole (NT), were designed and synthesized to investigate the impact of the variation in electron-deficient units on the properties of these photovoltaic polymers. It was exhibited that the down-shifted highest occupied molecular orbital energy level (E_{HOMO}), the enhanced aggregation in both the chlorobenzene solution and the solid film, as well as the better molecular planarity, were achieved using methods involving fluorination and the replacement of BT with NT on the polymer backbone. The absorption profile was little changed upon fluorination; however, it was greatly broadened during replacement of BT with NT. Consequently, the optimized photovoltaic device based on the PDTBDT-TIPS-DTNT-OD exhibited synchronous enhancements in the open-circuit voltage (V_{OC}) of 0.88 V, the short-circuit current density (J_{SC}) of 7.21 mA cm^{-2}, and the fill factor (*FF*) of 52.99%, resulting in a drastic elevation in the PCE by 129% to 3.37% compared to that of the PDTBDT-TIPS-DTBT-OD. This was triggered by PDTBDT-TIPS-DTNT-OD's broadened absorption, deepened E_{HOMO}, improved coplanarity, and enhanced SCLC mobility (which increased 3.9 times), as well as a favorable morphology of the active layer. Unfortunately, the corresponding PCE deteriorated after incorporating fluorine into the BT, due to the oversized aggregation and large phase separation morphology in the blend films, severely impairing its J_{SC}. Our preliminary results demonstrated that the replacement of BT with NT in a D-π-A type polymer backbone was an effective strategy of tuning the molecular structure to achieve highly efficient polymer solar cells (PSCs).

Keywords: TIPS-substituted dithienobenzodithiophene; modulating the electron-deficient units; naphtho[1,2-*c*:5,6-*c*′]bis[1,2,5]thiadiazole; fluorination; photovoltaic property

1. Introduction

Solar energy has gained considerable attention because it is considered environmentally friendly, is inexhaustible, and has a widespread distribution [1,2]. State-of-the-art bulk heterojunction (BHJ) polymer solar cells (PSCs), composed of conjugated polymers (CPs) as donors and fullerene derivatives as acceptors, can directly convert sunlight into electricity energy. This has led to a focus on PSCs because they possess unique merits, including low-cost fabrication of large-area devices, light weight, mechanical flexibility, and easy tunability of the PSCs chemical properties [3–5]. Recently, increased efforts have been devoted towards boosting the development of PSCs, where power conversion efficiencies (PCEs) in the single-junction have reached up to 11–13% [5–8]. However, in terms of commercialization, further improvement to the PCE is still needed, which can be achieved by developing efficient polymer donors for the BHJ photoactive layers. One of the most efficient methods for elevating the PCE is the development of low band gap (LBG) CPs, which can harvest more sunlight to generate a large short-circuit current (J_{SC}), theoretically, in the visible and near infrared (IR) regions [4,9–11]. Meanwhile, a deeper highest occupied molecular orbital (HOMO) energy level (E_{HOMO}) of donor CPs and a suitable lowest unoccupied molecular orbital (LUMO) energy level (E_{LUMO}) of the fullerene acceptor, can ensure a high open-circuit voltage (V_{OC}) and efficient exciton dissociation at the polymer/fullerene interface, respectively [12,13]. Moreover, constructing a planar molecular skeleton is of great importance and significance to obtain a closer π–π stacking, which can adjust the internal aggregation, charge transfer ability, and molecular conjugation [2]. Furthermore, it is essential to have appropriate compatibility with the fullerene acceptor to form a nanoscale bicontinuous interpenetration network to facilitate efficient charge generation and transport [14,15]. To address these goals, it is well established that the most popular and successful strategy is the incorporation of electron rich moieties (D) and electron deficient moieties (A), and alternating them onto the backbone. This can effectively influence the optical property and band gap, electronic energy levels, charge mobility, crystallinity, and morphology to promote the V_{OC}, J_{SC}, and the fill factor (*FF*) of the devices, and hence the PCE by selecting suitable D and A units and fine modulating the intramolecular charge transfer (ICT) interaction [16,17]. Nevertheless, the judicious selection of appropriate D and A units for constructing efficient donor CPs is still a great challenge.

Amongst the numerous A building blocks reported, benzo[*c*][2,1,3]thiadiazole (BT) containing a 1,2,5-thiadiazole ring and a strong *o*-benzoquinoidal unit has been extensively focused on owing to its easy synthesis, outstanding electro-withdrawing ability, and compact planar structure, which are conducive to the electron delocalization in the CPs after BT is incorporated into the polymer backbone [18–21]. With these good features, excellent D–A photovoltaic (PV) CPs containing BT, such as PCDTBT [22], PCPDTBT [23], PBTz4T [5,14,24], PffBT4T-2OD [5], PBDT-DTBT [25], and PDTBDT-BT [26], have been widely investigated. Moreover, incorporating fluorine (F) onto the BT has also proven to be an effective and facile strategy when targeting efficient PSCs, which can effectively down-shift the energy level without sacrificing the bandgap owing to the electronegative element of the F atom with a Pauling electronegativity of 4.0, reducing the undesirable steric hindrance due to the relatively small van der Walls radius (147 pm), as well as promoting the fascinating molecular ordering assisted by the inter- and intra-molecular C–F···H, F···S, and C–F···π_F interaction. Therefore, this accelerates the exciton dissociation and increases the lifetime of the charge carrier by reducing the Coulombic interaction between the electron–hole by virtue of the induced dipole [27–36]. The fluorination had different effects on the absorption properties in different CPs systems, including blue-shift [37–40], without change [41–44], and red-shift [45,46]. What cannot be ignored is that fluorination can improve the coplanarity of the molecular backbone in CPs, and it further improves the charge mobility; however, it inevitably reduces the solubility of CPs to restrict the solution-processed fabrication [40]. As an alternative, an emerging centrosymmetric naphtho-[1,2-*c*:5,6-*c*′]bis[1,2,5]thiadiazole (NT), with an extended conjugation, an enlarged planarity, and a stronger electron-withdrawing ability due to the existence of doubly fused 1,2,5-thiadiazole rings relative to the axisymmetric BT, exhibited interesting electronic properties and a high self-assembling

nature [7,21,24,25,40,47–50]. Early in 2011, Huang et al. first incorporated NT into the polymer backbone and combined it with alkylthienyl-substituted benzo[1,2-*b*:4,5-*b*′]dithiophene (BDT) to develop PBDT-DTNT, showing an obviously extended absorption profile, which had a one order of magnitude higher charge mobility and a 2.84 times higher PCE compared to its BT-based counterpart PBDT-DTBT, even if the decreased V_{OC} (0.8 V *vs*. 1.0 V) originated from an elevated E_{HOMO} [25]. After that, Osaka et al. combined NT with oligothiophene, and the designed PNTz4T exhibited a narrower bandgap, a deeper E_{HOMO}, a more highly ordered structure, and a 2.48 times increase in the PCE, compared to those of its counterpart PBTz4T [24]. Xu et al. further introduced 4,9-di(thien-2-yl)naphthobisthiadiazole (DTNT) and 4,7-dithienyl-benzothiadiazole (DTBT) as a 2D conjugated side chain into the BDT-based polymer backbone, and found that PBDTT-TANT could induce a stronger ICT effect between the polymer backbone and the NT-based conjugated side chain. Additionally, an overtly broadened absorption spectra and a tighter molecular stacking structure were achieved, and thus the J_{SC}, *FF*, and PCE correspondingly improved from 11.12 to 13.06 mA cm^{-2}, 62.1% to 65.2%, and 6.74% to 8.04%, respectively, despite a lower V_{OC} value [50]. These results confirmed that the replacement of BT with NT was a facile and effective strategy and it was expected to broaden the absorption, tune the energy level, and optimize the film morphology, thereby promoting the PV performance.

Recently, large heteroacenes have been employed in efficient PSCs, as they provide several advantages, including improved charge mobility originating from the increased interchain π–π stacking assisted by large planar π-conjugated structures [51]. In addition, an increased effective conjugation length in heteroacenes-containing CPs is expected to minimize the Marcus reorganization energy of the polymer system to facilitate exciton separation into free charge carriers [51–58]. Specifically, dithieno[2,3-*d*:2′,3′-*d*′]benzo[1,2-*b*:4,5-*b*′]dithiophene (DTBDT) has proven to be an excellent building block in the PSCs field [59–63]. Furthermore, bulk triisopropyl-silylethynyl (TIPS) on heteroacenes not only improve the solubility, crystallinity, and oxidative stability of semiconductors, but they also promote the π-orbital overlap between conjugated molecules [17,54,59–63]. In 2013, Kim and a co-worker introduced TIPS into BDT, where they prepared two benzo[*d*][1,2,3]triazole-based copolymers, and demonstrated that TIPS could not only effectively deepen the E_{HOMO} from −5.26 to −5.40 eV and correspondingly elevate the V_{OC} from 0.77 to 0.80 V, but they could also impel formation of a crystalline lamellar structure to enhance the hole mobility and increase the J_{SC} (12.69 vs. 7.87 mA cm^{-2}), *FF* (55% vs. 48%), and PCE (5.53% vs. 2.88%) of the devices [61]. Afterwards, our group designed a different side chain alkyloxy (OR), alkylthienyl, and TIPS onto a DTBDT moiety, and we also found that a DTBDT-TIPS-based CP yielded the best PCE of 6.39% via simultaneous enhancements in the V_{OC}, J_{SC} and *FF* [54].

Prompted by the abovementioned considerations, this study focused on three D-π-A type CPs, PDTBDT-TIPS-DTBT-OD, PDTBDT-TIPS-DTFBT-OD, and PDTBDT-TIPS-FTNT-OD (Figure 1), in which TIPS-substituted DTBDT (DTBDT-TIPS) was selected as the D moiety, electron-withdrawn BT, 5,6-difluoro-BT (FBT) and NT units were selected as the A unit, and the long branched 2-octyldodecyl groups introduced the thiophene segment as conjugated π bridges for guaranteeing sufficient solution-processability. These components were designed and prepared to study the preliminary influence of the variation of the A unit on the photophysical, electrochemical, aggregation, and PV performances. The impacts of fluorination and the replacement of BT with NT on the absorption spectra, molecular energy levels, aggregation ability, backbone planarity, and mobility via tuning of the A moieties, resulted in the optical band gaps (E_g^{opt}), E_{HOMO}, and E_{LUMO}, correspondingly varying in the ranges of 1.83~1.67 eV, −5.35~−5.46 eV, and −3.46~−3.66 eV, respectively. The absorption profile was slightly blue-shifted by the fluorination; however, it was greatly broadened after replacing the BT with NT, and the E_{HOMO} was deepened. It was revealed that PDTBDT-TIPS-DTNT-OD exhibited the best PCE of 3.37%, which was 1.29 times higher than its counterpart PDTBDT-TIPS-DTBT-OD, where such an improvement originated from the broadened absorption, lower E_{HOMO}, and an

optimized morphology. Unfortunately, the PCE decreased by 25.9% from fluorination, because of an oversized aggregation morphology and suppressed J_{SC}, despite a high V_{OC} of 0.93 V.

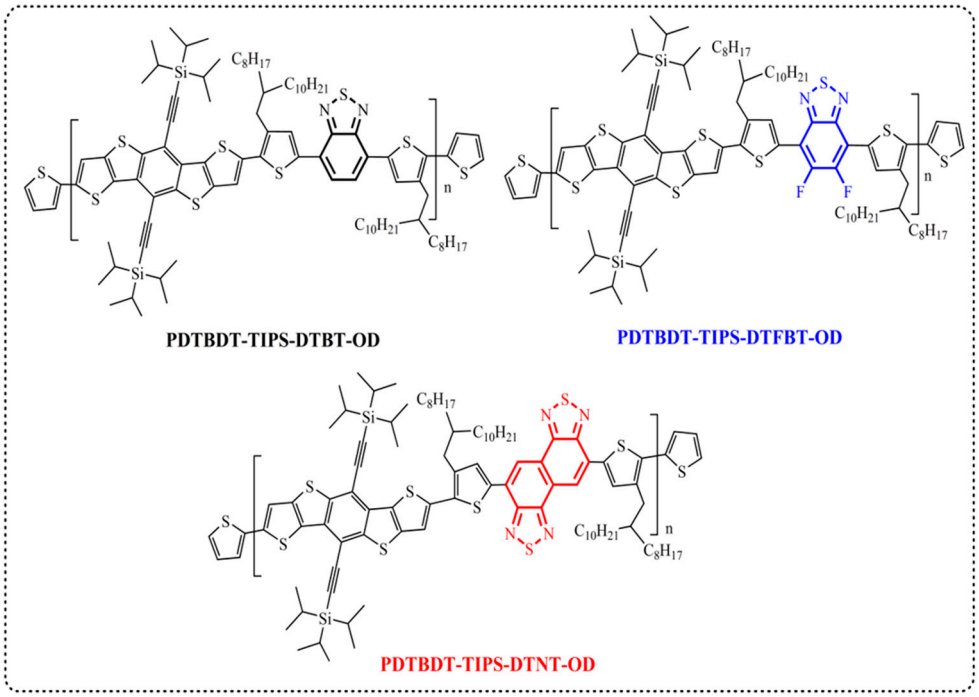

Figure 1. The structures of the studied copolymers.

2. Materials and Methods

2.1. Characterization

^{1}H nuclear magnetic resonance (^{1}H NMR) and ^{13}C NMR spectra were measured on a Bruker DRX 600 (Rheinstetten, Germany) 600 MHz and 126 MHz spectrometer, respectively, with tetramethylsilane (TMS) as the internal reference. The chemical shifts were recorded in units of ppm and the splitting patterns were designed as s (singlet), d (doublet), t (triplet), m (multiplet), and br (broaden). Melting points were obtained on a microscopic melting point apparatus (Beijing Taike, Beijing, China), and the temperature gauge was uncorrected. C, H, and N elemental analyses (EAs) were carried out on a Vario EL Elemental Analysis Instrument (Elementar Co., Hanau, Germany). TGA curves were collected on TGA 2050 instruments (New Castle, DE, USA), at the heating rate of 10 °C min^{-1} and under an N_2 flow rate (20 mL min^{-1}). Polymer molecular weights were obtained using a Waters GPC 2410 in relative to polystyrene standards utilizing THF as the eluent. UV-Vis absorption measurement was performed on a UV-1800 spectrophotometer (Shimadzu, Kyoto, Japan). Thin film X-ray diffraction (XRD) was recorded on a PANalytical X'Pert PRO diffractometer (PANalytical Inc., Almelo, the Netherlands) equipped with a rotating anode (Cu Ka radiation, λ = 1.54056 Å). The electrochemical properties of the polymer films were measured on a CHI600D electro-chemical instrument (Shanghai Chenhua, Shanghai, China) in anhydrous CH_3CN, at a scan rate of 100 mV s^{-1} under N_2. Tetra(*n*-butyl)ammonium hexafluorophosphate (Bu_4NPF_6) (0.1 mol L^{-1}) was utilized as the electrolyte. A three-electrode cell was used in all the experiments, wherein a glassy carbon electrode coated with polymer film, platinum wire, and an $Ag/AgNO_3$ (0.01 mol L^{-1} of $AgNO_3$ in CH_3CN) electrode were used as the working, counter, and reference electrodes, respectively. The potential of the $Ag/AgNO_3$ reference electrode was calibrated using the ferrocene/ferrocenium couple (Fc/Fc^+), where the energy level was −4.80 eV. Note that the polymer thin films were obtained by drop casting 1 μL polymer chloroform solution, with a concentration of 1 mg mL^{-1}, onto the glass carbon electrode, and then it was dried in air. Atomic force microscopy (AFM) images (5 × 5 μm^2) were acquired on an MFP-3D-SA (Asylum Research,

Santa Barbara, CA, USA) in a tapping mode. Transmission electron microscopy (TEM) images were acquired with a Tecnai G^2 F20 (FEI, Hillsboro, OR, USA) transmission electron microscope at an accelerating voltage of 200 kV.

2.2. Materials

All reagents were purchased from commercial sources (Sigma-Aldrich (Shanghai), Shanghai, China; Acros, Belgium, USA; J&K, Beijing, China; and TCI (Shanghai), Shanghai, China), and were used as received without further purification, unless otherwise stated. THF and Et_2O were distilled from sodium/benzophenone and were freshly distilled before use. The conjugated polyelectrolyte material PFN, which utilized was as an electron-interface layer as in Reference [64], and dibromide 4,9-bis(5-bromo-4-(2-octyldodecyl)thien-2-yl)naphtho[1,2-*c*:5,6-*c*′]bis[1,2,5]thiadiazole (DTNT- $ODBr_2$) [65], were synthesized according to the reported methods. The synthetic routes of the dibromides 4,7-bis(5-bromo-4-(2-octyl-dodecyl)thien-2-yl)benzo[*c*][1,2,5]thiadiazole (DTBT-$ODBr_2$), the 4,7-bis- (5-bromo-4-(2-octyldodecyl)thien-2-yl)-5,6-difluorobenzo[*c*][1,2,5]thiadiazole (DTFBT-$ODBr_2$), and the bistin 2,7-bis(trimethyltin)-5,10-bis(triisopropylsilylethynyl)dithieno[2,3-*d*:2′,3′-*d*′]benzo[1,2-*b*:4,5-*b*′]-dithiophene (DTBDT-TIPSSn) as described in Reference [54], were seen in the Supporting Information.

2.3. Polymer Synthesis

The general procedure adopted for polymer synthesis was as follows: Carefully purified bistin monomer DTBDT-TIPSSn and dibromo-monomer (DTBT-$ODBr_2$, DTFBT-$ODBr_2$, and DTNT-$ODBr_2$) were dissolved into 6 mL degassed dry toluene and 0.8 mL DMF in a 25 mL two-neck round-bottom flask under argon (Ar) conditions. The mixture was bubbled with Ar for another 20 min to remove O_2. Thereafter, $Pd_2(dba)_3$ (1.4 mg), P(o-tolyl)$_3$ (2.3 mg) were quickly added to the mixture in one portion and the solution was bubbled with Ar for another 20 min. The mixture was then vigorously refluxed for 48 h under Ar, followed by the subsequent addition of 2-tri(butylstannyl)thiophene and 2-bromothiophene at an interval of 8 h for ending-capping. After further reflux at 8 h, the mixture was poured into 300 mL methanol. The precipitate was collected by filtration and the crude polymer was subjected to Soxhlet extraction successively with ethanol, acetone, hexane, and toluene. The toluene fraction was condensed to about 6 mL and precipitated into methanol. The black solid was collected and completely dried under vacuum overnight to obtain the target material with a yield of 56.9%~81.2%

2.3.1. Poly[5,10-bis(triisopropylsilylethynyl)dithieno[2,3-*d*:2′,3′-*d*′]benzo[1,2-*b*:4,5-*b*′]dithiophene-2,7-diyl-*alt*-4,7-bis(4-(2-octyldodecyl)thien-2-yl)benzo[*c*][1,2,5]thiadiazole-5,5′-diyl] (PDTBDT-TIPS-DTBT-OD)

DTBDT-TIPSSn (100.9 mg, 0.102 mmol) and DTBT-$ODBr_2$ (104.0 mg, 0.102 mmol) were used to prepare the PDTBDT-TIPS-DTBT-OD according to the general procedure illustrated above. A black solid of 101.6 mg was obtained with a yield of 65.5%. Number-average molecular weights (M_n) = 13.4 kDa, polydispersity index (PDI) = 1.80. ^{1}H NMR (600 MHz, $CDCl_3$), δ (ppm), 8.03 (m, ArH), 7.84 (m, ArH), 7.62 (m, ArH), 7.44 (m, ArH), 7.07 (m, ArH), 2.91 (br, CH_2), 1.97 (br, CH), 1.80–0.7 (m, CH, CH_2, CH_3). Anal. Calcd for $C_{90}H_{130}N_2S_7Si_2$: C, 71.09%; H, 8.62%; N, 1.84%. Found, C, 71.00%; H, 8.50%; N, 1.95%.

2.3.2. Poly[5,10-bis(triisopropylsilylethynyl)dithieno[2,3-*d*:2′,3′-*d*′]benzo[1,2-*b*:4,5-*b*′]dithiophene-2,7-diyl-*alt*-4,7-bis(4-(2-octyldodecyl)thien-2-yl)-5,6-difluorobenzo[*c*][1,2,5]thiadiazole-5,5′-diyl] (PDTBDT-TIPS-DTFBT-OD)

DTBDT-TIPSSn (97.0 mg, 0.098 mmol) and DTFBT-$ODBr_2$ (103.0 mg, 0.098 mmol) were used to prepare the PDTBDT-TIPS-DTFBT-OD according to the general procedure illustrated above. A black solid of 86.8 mg was obtained with a yield of 56.9%. M_n = 14.4 kDa, PDI = 1.90. ^{1}H NMR (600 MHz, $CDCl_3$), δ (ppm), 8.15 (m, ArH), 7.93 (m, ArH), 7.61 (m, ArH), 7.50 (m, ArH), 7.37 (m, ArH), 7.13

(m, ArH), 2.88 (br, CH_2), 1.90 (br, CH), 1.40–1.10 (m, CH, CH_2), 0.77 (t, CH_3). Anal. Calcd for $C_{90}H_{1280}F_2N_2S_7Si_2$: C, 69.44%; H, 8.291%; N, 1.80%. Found, C, 69.01%; H, 8.51%; N, 1.90%.

2.3.3. Poly[5,10-bis(triisopropylsilylethynyl)dithieno[2,3-*d*:2′,3′-*d*′]benzo[1,2-*b*:4,5-*b*′]dithiophene-2,7-diyl-*alt*-4,9-bis(4-(2-octyldodecyl)thien-2-yl)naphto[1,2-*c*:5,6-*c*′]bis[1,2,5]thiadiazole-5,5′-diyl] (PDTBDT-TIPS-DTNT-OD)

DTBDT-TIPSSn (102.9 mg, 0.104 mmol) and DTNT-ODBr$_2$ (117.4 mg, 0.104 mmol) were used to prepare the PDTBDT-TIPS-DTNT-OD according to the general procedure illustrated above. A black solid of 137.6 mg was obtained with a yield of 81.2%. M_n = 13.6 kDa, PDI = 1.94. ^{1}H NMR (600 MHz, $CDCl_3$), δ (ppm), 9.05 (m, ArH), 7.93 (m, ArH), 8.39 (br, ArH), 8.02 (m, ArH), 7.74 (m, ArH), 7.37 (m, ArH), 7.01 (m, ArH), 6.73 (m, ArH), 2.91 (br, CH_2), 2.04 (br, CH), 1.40–1.10 (m, CH, CH_2), 0.85 (m, CH_3). Anal. Calcd for $C_{94}H_{130}N_4S_8Si_2$: C, 69.32%; H, 8.04%; N, 3.44%. Found, C, 69.20%; H, 8.01%; N, 3.47%.

2.4. Fabrication and Characterization of the PSCs

A patterned indium tin oxide (ITO) coated glass with a sheet resistance of 10–15 Ω/square was sequentially cleaned using detergent, deionized water, acetone, and *iso*-propanol in an ultrasonic cleaner. Solar cell devices were fabricated using an inverted configuration of the ITO/PFN/active layer/MoO_3/Ag. Note that the interlayer PFN layer was prepared according to the reported method described in Reference [65]. The active layer, with a thickness in the 90–110 nm range, was deposited on top of the interlayer layer by spin-casting from the chlorobenzene (CB) solution containing the studied copolymers/$PC_{61}BM$ (*w*/*w*; 1:1, 1:1.5, and 1:2), respectively. The thickness of the photosensitive layer was approximately 80–120 nm, detected on a surface profilometer (DektakXT, Bruker, MA, USA). A MoO_3 layer with a thickness of about 8 nm was thermally evaporated at an evaporation rate of 0.1 Å s^{-1}, at a vacuum degree of 5 × 10^{-5} Pa. At the end of the fabrication process, the Ag layer (100 nm) was evaporated by a shadow mask. The overlapping area between the cathode and anode was defined by a pixel size of 0.10 cm^2. The thickness of the hole-transporting MoO_3 layer and the metal Ag electrode, were both monitored using a quartz crystal thickness/ratio monitor (SI-TM206, Shenyang Sciens Co., Shenyang, China). All the fabrication processes were finished in a nitrogen drybox (Etelux Co., Beijing, China), where its contents of oxygen and moisture were both less than 1 ppm. The current density–voltage (*J*–*V*) curves were measured on a Keithley 2400 source-measurement unit. The PCEs of the PSCs were measured under a 1 sun, AM 1.5 G (Air mass 1.5 global) spectrum using a XES-70S1 (San-EI Electric Co. Ltd., Osaka, Japan) solar simulator (AAA grade), with an irradiation of 100 mW cm^{-2}. The external quantum efficiency (EQE)/incident photon to charge carrier efficiency (IPCE) was obtained on a 7-SCSpecIII Solar Cell Spectral Response Measurement System (Beijing 7-star Opt. In. Co., Beijing, China), and the absolute photosensitivity was determined using a calibrated silicon detector.

2.5. Hole-Only Device Fabrication and Measurement

The hole mobility of the active layer was measured from the J–V curves obtained under dark current using the steady state space charge-limited current (SCLC) method, with the hole-only device configuration of the ITO/PEDOT:PSS/active layer/MoO_3/Ag. The processing conditions for the active layers were the optimized one. The J–V curves were fitted using the Mott-Gurney square law as References [65,66]: $J = \frac{9}{8}\varepsilon_0\varepsilon_r\mu\frac{V^2}{L^3}$, where J is the current density, ε_0 is the free space permittivity (8.85 × 10^{-12} F m^{-1}), ε_r is the dielectric constant of the polymer (assumed to be 3), μ is the hole mobility, L is the thickness of the BHJ active layer film, and the effective potential $V = (V_{appl} - V_{bi})$: where V_{appl} is the applied potential and V_{bi} is the built-in voltage resulting from difference in the work function of the anode and cathode. Finally, the mobility was extracted from the slope and L according to $\mu = \frac{slope^2 \times 8L^3}{9\varepsilon_0\varepsilon_r}$, by linearly fitting $J^{1/2}$ with V.

3. Results

3.1. Molecular Design, Synthesis, and Characterization

Synthetic pathways for dibromide DTBT-ODBr$_2$, DTFBT-ODBr$_2$, and bistin comonomer DTBDT-TIPSSn [54], are outlined in Schemes S1 and S2 in the supporting information. The structures and purity of all the compounds were fully characterized and identified by ^{1}H NMR (Figures S1–S6) and elemental analysis. The DTNT-ODBr$_2$ was synthesized according to our reported procedure in Reference [65]. As depicted in Scheme 1, three target CPs, PDTBDT-TIPS-DTBT-OD, PDTBDT-TIPS-DTFBT-OD, and PBDT-TIPS-DTNT-OD bearing different A units, were prepared using a typical Stille polymerization reaction between the bistin DTBDT-TIPSSn and the dibrominated DTBT-ODBr$_2$, DTFBT-ODBr$_2$, and DTNT-ODBr$_2$ in toluene, with the use of tri(dibenzylidene-acetone)dipalladium(0) [Pa$_2$(dba)$_3$] as a catalyst and tri(*o*-tolyl)phosphine [P(*o*-tol)$_3$] as a ligand as described in Reference [67]. Note that, to improve the stability of the copolymers, the end-capping was performed with 2-tributyl-stannylthiophene and 2-bromothiophene as in Reference [22]. The product polymers were purified by Soxhlet extractions using ethanol, acetone, hexane, and toluene as the eluent to remove oligomers and catalyst impurities. Ultimately, the toluene-soluble fraction was recovered by being reprecipitated in methanol and then dried under vacuum overnight to remove the residual solvents. These copolymers were obtained as black solids with yields of 56.9%~81.2%. PDTBDT-TIPS-DTBT-OD and PDTBDT-TIPS-DTNT-OD possessed good solubility in common organic solvents, such as chloroform (CF), CB, and *o*DCB at an ambient temperature. However, fluorinated PDTBDT-TIPS-DTBT-OD exhibited limited solubility, except for at an elevated temperature. The ^{1}H NMR spectra of these studied copolymers are shown in Figures S7–S9. M_n and PDIs values were estimated to be 13.4 kDa and 1.80 for PDTBDT-TIPS-DTBT-OD; 14.4 kDa and 1.90 for PDTBDT-TIPS-DTFBT-OD; and 13.6 kDa and 1.94 for PDTBDT-TIPS-DTNT-OD, respectively, Table S1 implies that the effect caused by different molecular weights could be ignored. The thermal properties of these copolymers were evaluated by thermogravimetry analysis (TGA) under a nitrogen atmosphere. As shown in Figure S10, the decomposition temperatures (T_d) at a 5% weight-loss ranged from 352 to 387 °C (Table S1), suggesting that the studied CPs possessed adequate thermal stability for the fabrication of PSCs.

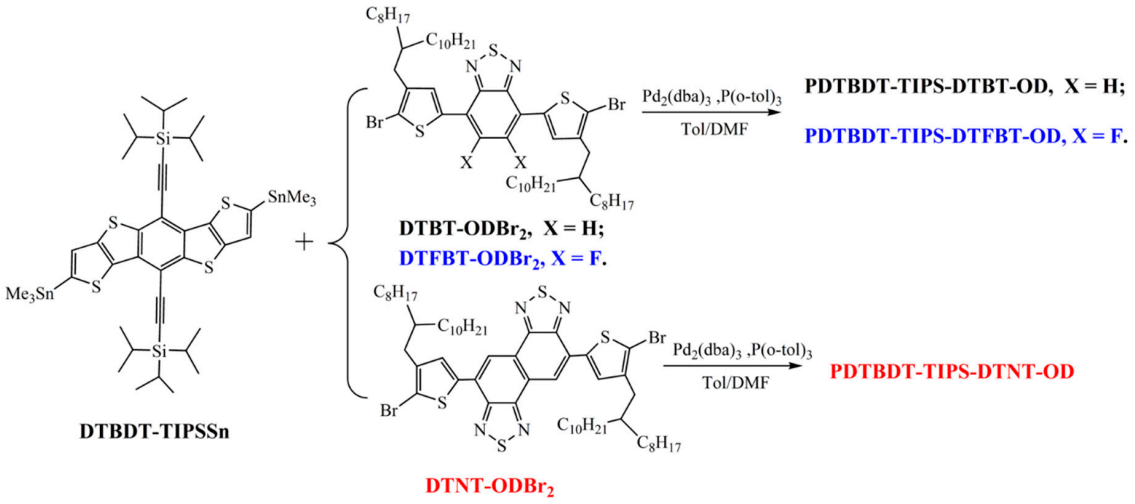

Scheme 1. The synthetic route of copolymers.

3.2. Optical Property

The effect of the electro-withdrawing of fluorine onto BT and the replacement of BT with NT on absorption was investigated in both the CB solutions and as solid films. Normalized UV-Vis absorption spectra are elucidated in Figure 2, and the detailed parameters are summarized in Table 1.

The absorption profile of PDTBDT-TIPS-DTBT-OD was similar to the analogue PTBDT-BT [17]. The absorption peaks at the high energy region are ascribed to the π–π* transition from the main chain units of the polymer backbone, while ones at low energy region are caused by the ICT transition [68]. Obviously, in the CB solution, the maximum absorption peak was blue-shifted by 17 nm from 552 to 535 nm by the fluorination, but a dramatic red-shift value of approximately 80 nm and one distinct shoulder peak were observed after incorporating NT into the polymer backbone, suggesting that there existed a stronger interaction even in the diluted solution as in Reference [25]. Going from solution to film state, the red-shifted values of the maximum absorption peaks were 30, 47, and 3 nm for the PDTBDT-TIPS-DTBT-OD, PDTBDT-TIPS-DTFBT-OD, and PBDT-TIPS-DTNT-OD, respectively. We also observed that there existed weaker shoulder peaks at about 620 nm for the former two BT-based CPs, and the blue-shifted value of 14 nm of the shoulder peak for PBDT-TIPS-DTNT-OD. The optical bandgaps (E_g^{opt}) of the films for the copolymers could be estimated using the absorption edge (λ_{onset}^{film}), according to the empirical equation $E_g^{opt} = 1240/\lambda_{onset}^{film}$, and accordingly the E_g^{opt}s were calculated as 1.82, 1.83, and 1.67 eV for the PDTBDT-TIPS-DTBT-OD, PDTBDT-TIPS-DTFBT-OD, and PBDT-TIPS-DTNT-OD, respectively. Plainly, the E_g^{opt} was almost unaffected by the fluorination, but it was effectively reduced by replacing the BT with NT. Apart from the absorption profile, the absorption coefficient was also a pivotal parameter in judging the ability to harvest solar light of CPs [69]. Therefore, the corresponding absorption coefficients in both the CB (Figure S11) and film (Figure S12) were tested, and PBDT-TIPS-DTNT-OD exhibited the highest coefficient at the maximum absorption in film (ε_{max}^{film}), and the fluorination decreased the corresponding absorption coefficients (Table S2). It was inferred that NT-based CP could harvest more sunlight which was propitious to achieve a good J_{SC}.

Table 1. Optical and electrochemical characteristics of copolymers.

Polymer	Solution		Film			E_g^{opt} [1] (eV)	φ_{ox}^{onset} (V)	φ_{red}^{onset} (V)	E_{HOMO} [2] (eV)	E_{LUMO} [3] (eV)	E_g^{ec} [4] (eV)
	λ_{max} (nm)	λ_{sh} (nm)	λ_{max} (nm)	λ_{sh} (nm)	λ_{onset} (nm)						
PDTBDT-TIPS-DTBT-OD	366,425,552	–	375,582	620	680	1.82	0.67	−1.22	−5.35	−3.46	1.89
PDTBDT-TIPS-DTFBT-OD	365,427,535	–	375,582	622	678	1.83	0.78	−1.14	−5.46	−3.54	1.92
PDTBDT-TIPS-DTNT-OD	361,402,632	692	363, 405,492, 635	678	740	1.67	0.75	−1.02	−5.43	−3.66	1.77

[1] Optical band gap determined from the UV-vis absorption onset of the film ($E_g^{opt} = 1240/\lambda_{onset}^{film}$). [2] Calculated from the oxidation potential of the copolymer ($E_{HOMO} = -e(\varphi_{ox}^{onset} + 4.68)$ (eV)). [3] Calculated from the reduction potential of the copolymer ($E_{LUMO} = -e(\varphi_{red}^{onset} + 4.68)$ (eV). [4] Calculated from the equation $E_g^{ec} = e(\varphi_{ox}^{onset} - \varphi_{red}^{onset})$ (eV).

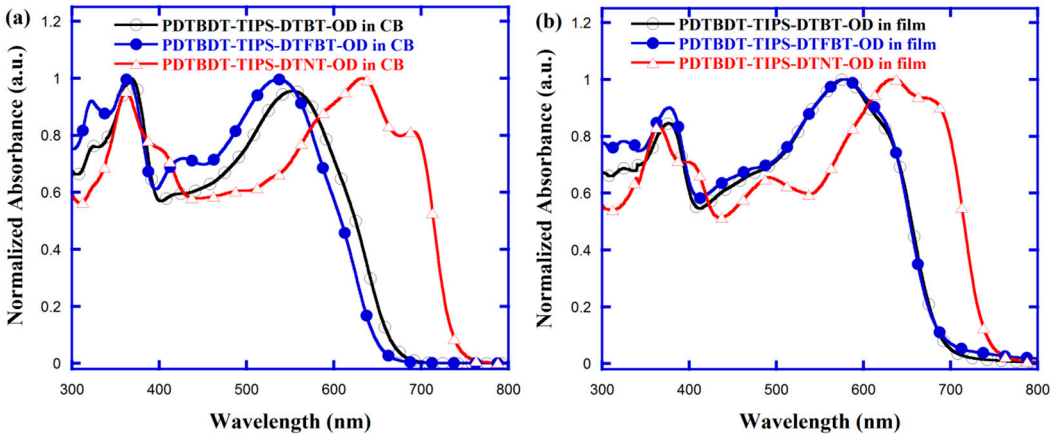

Figure 2. Normalized UV-vis absorption spectra of copolymers in diluted chlorobenzene (CB) solution of approximately 10^{-5} mol L^{-1} (**a**) and thin film state (**b**).

It has been confirmed that with rising temperature the molecule motions of CPs are bound to be accelerated, resulting in a reduction of the absorption shoulder peaks with regard to the aggregation

evoked by intermolecular π–π* transition. Namely, the distortion of the conjugated backbone is strengthened at the elevated temperature, leading to a decrease of the effective conjugation length of the polymer backbone, and hence the absorption peaks engendered by the localized π–π* transitions, and the ones emerged from ICT transitions are both blue-shifted [49,70]. To gain insight into the difference between fluorination and the replacement of BT with NT on the interchain π–π stacking in solution, temperature-dependent absorption (TD-Abs) spectra of these copolymers in CB solution were measured, as shown in Figure 3. It was exhibited that as the temperature increased from 25 °C to 105 °C, the ICT absorption peaks (0–0 peak for the BT-based CPs and 0–1 peak for the NT-based CP) were all blue-shifted and the absorption strength decreased. In detail, the blue-shifted values (Δλ) and the decreased absorption strength (ΔA) were 20 nm and 3.88% for PDTBDT-TIPS-DTBT-OD; 15 nm and 3.20% for PDTBDT-TIPS-DTFBT-OD; and 62 nm and 7.47% for PDTBDT-TIPS-DTNT-OD, respectively. Furthermore, the absorption peak (0–0 peak) related to the aggregation was only observed in the PDTBDT-TIPS-DTNT-OD and it showed a trend of blue-shifting and decreasing, and it completely disappeared until the temperature was heated to 65 °C. As observed from the results, the order of aggregation ability in the CB solution should be: PDTBDT-TIPS-DTNT-OD > PDTBDT-TIPS-DTFBT-OD > PDTBDT-TIPS-DTBT-OD [70].

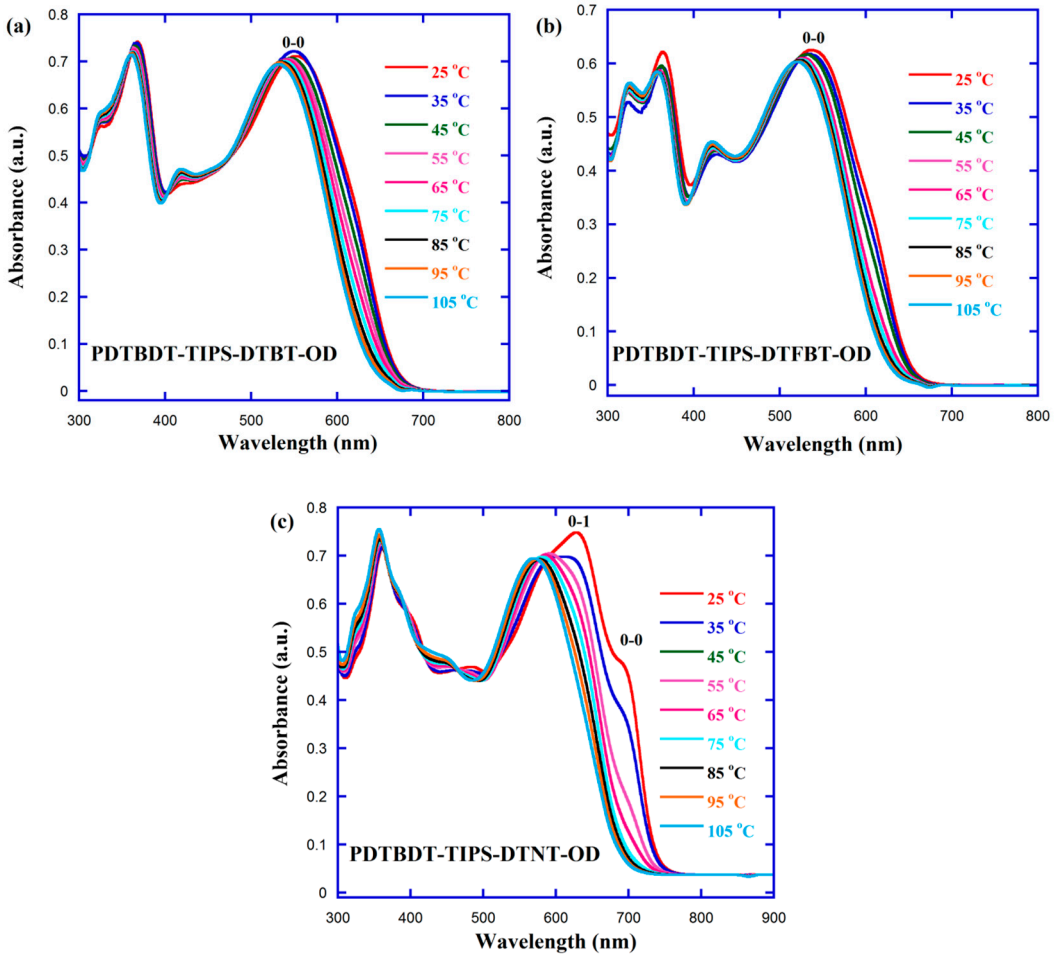

Figure 3. TD-Abs spectra for polymers in the CB with the concentration of approximately 10^{-5} mol L^{-1} (temperature ranged from 105 to 25 °C with a 10 °C interval).

3.3. X-Ray Diffraction (XRD) Analysis

To get a deeper perspective on the impact of fluorination and the substitution of BT with NT on intermolecular interaction in the film state, X-ray diffraction (XRD) was adopted to investigate the formation of ordered structures within these studied polymers. The preparation conditions for these

pristine polymer films was casted from polymer CB solution onto glass substrate. As illustrated in Figure 4, all copolymers exhibited two discernible peaks. The first peaks in a small angle region were located at 2θ of 4.00° for PDTBDT-TIPS-DTBT-OD, 4.08° for PDTBDT-TIPS-DTFBT-OD, and 4.25° for PDTBDT-TIPS-DTNT-OD, such that the distance of the polymer backbone separated by the flexible side was 22.06, 21.63, and 20.77 Å, respectively, based on the Bragg's law (i.e., λ = 2dsinθ) [71]. The broad diffraction peaks at the wide-angle region, which reflects the π–π stacking distance, were located at 2θ of 20.62° for PDTBDT-TIPS-DTBT-OD, 2θ of 20.91° for PDTBDT-TIPS-DTFBT-OD, and 23.25° for PDTBDT-TIPS-DTNT-OD, respectively, corresponding to π–π stacking distances of 4.30 Å, 4.24 Å, and 3.89 Å. It was inescapably clear that the order of aggregation in the solid film state was PDTBDT-TIPS-DTNT-OD > PDTBDT-TIPS-DTFBT-OD > PDTBDT-TIPS-DTBT-OD, which was in accordance with the previous one in the CB solution.

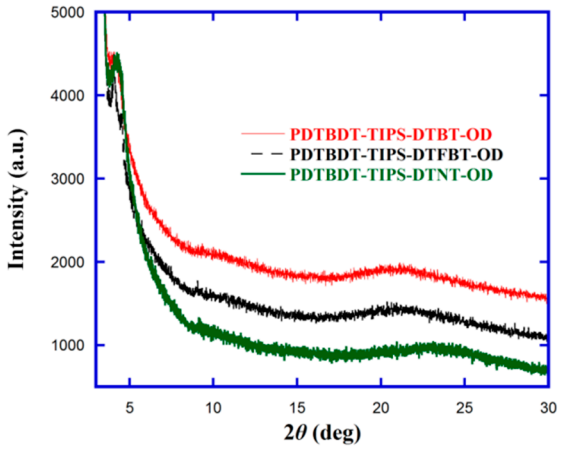

Figure 4. X-ray patterns of copolymers.

3.4. Electrochemical Property

It is well known that the E_{HOMO}, E_{LUMO}, and electrochemical bandgap (E_g^{ec}) of as-prepared CPs were important parameters in photovoltaic application. Therefore, the cyclic voltammetry (CV) method was applied to characterize the electrochemical properties, and the E_{HOMO} and E_{LUMO} were estimated from the oxidation onset potential (φ_{ox}^{onset}) and the reduction onset potential (φ_{red}^{onset}), respectively. The CV curves were recorded in Figure 5a, and the detailed data were listed in Table 1. Three CPs exhibited the quasi-reversible p-doping and n-doping processes, which were important for p-type semiconductor materials. We could see that the φ_{ox}^{onset}s for PDTBDT-TIPS-DTBT-OD, PDTBDT-TIPS-DTFBT-OD, and PDTBDT-TIPS-DTNT-OD were observed at around 0.67, 0.78, and 0.75 V, respectively. Note that the reference electrode was calibrated using the ferrocene–ferrocenium (Fc/Fc^+) redox couple, which had redox potential with an absolute energy level of −4.80 eV relative to the vacuum energy level [72]. Meanwhile, this potential $\varphi_{1/2}$ of the Fc/Fc^+ redox couple was found to be 0.12 V under the exact same conditions. Accordingly, the E_{HOMO} and E_{LUMO} were calculated from the following equation: $E_{HOMO} = -e(\varphi_{ox}^{onset} + 4.68)$ (eV) and $E_{LUMO} = -e(\varphi_{red}^{onset} + 4.68)$ (eV), where φ_{ox}^{onset} and φ_{red}^{onset} are the onset oxidation and/or the reduction potentials vs. $Ag/AgNO_3$, and the corresponding E_{HOMO}/E_{LUMO} values were approximately −5.35/−3.46 eV, −5.46/−3.54 eV, and −5.43/−3.66 eV for PDTBDT-TIPS-DTNT-OD, PDTBDT-TIPS-DTFBT-OD, and PBDT-TIPS-DTNT-OD, respectively. Clearly, the depressed E_{HOMO} values were 0.11 and 0.08 eV for fluorination and the replacement BT with NT, respectively, which were both prone to obtaining high a V_{OC} in the PSCs [4]. The E_g^{ec} was calculated from the equation $E_g^{ec} = e(\varphi_{ox}^{onset} - \varphi_{red}^{onset})$ (eV), and the E_g^{ec} values were 1.89, 1.92, and 1.77 eV for DTBDT-TIPS-DTNT-OD, PDTBDT-TIPS-DTFBT-OD, and PBDT-TIPS-DTNT-OD, respectively. These observed values were slightly higher (0.07–0.10 eV) than those of the E_g^{opt}, which presumably resulted from the exciton binding energies of the CPs and/or the interfacial barriers for charge injection [73]. For a better comparison, the energy levels diagram

of the three donor copolymers and $PC_{71}BM$ is described in Figure 5b. It could be inferred that all the polymers were suitable for use as donor materials to match well with the $PC_{71}BM$, which had LUMO gaps of 0.54~0.74 eV, exhibiting sufficient driving force to facilitate an exciton dissociation at the D–A interfaces, thereby guaranteeing energetically favorable electron transfer to overcome the binding energy of the intrachain exciton [11]. Interestingly, the replacement of BT with NT could simultaneously achieve the balance of deepening the E_{HOMO} and reducing the bandgap of the donor polymer, which differed from the observations in PBDT-DTNT [25] and PBDTT-TNAT [11]. This meant that an obviously decreased bandgap of the PDTBDT-TIPS-DTNT-OD principally benefited from the remarkably deepened E_{LUMO}.

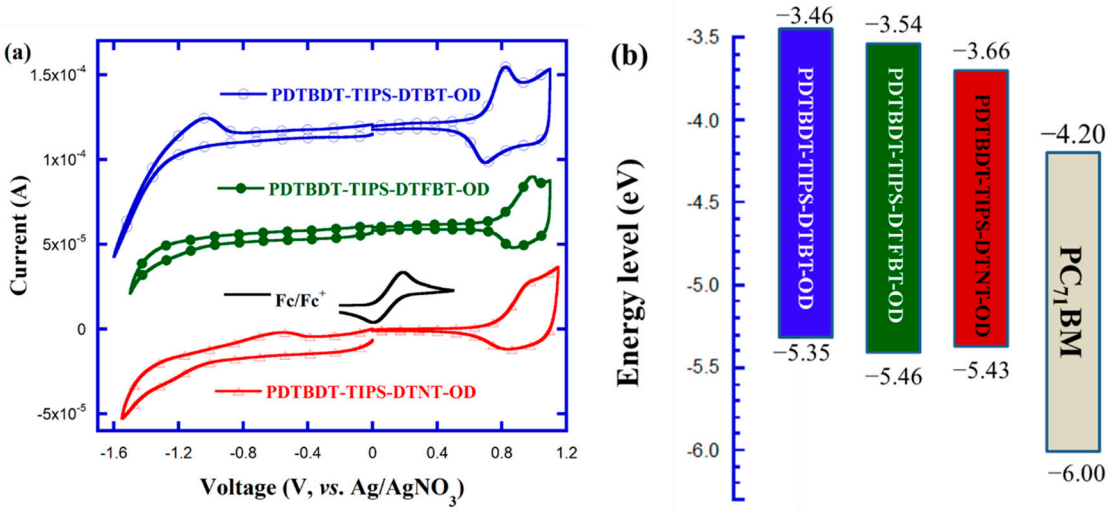

Figure 5. Cyclic voltammetry curves (**a**) and energy levels schematic diagram (**b**) of copolymers.

3.5. Theoretical Calculation

To further inspect the effect of fluorination and replacement of the BT with NT on the molecular backbone conformation and the electron density distributions, the calculations were carried out the using density functional theory (DFT) calculation on the B3LYP/6-31G* basis set, implemented in the Gaussian 09 program suite as in Reference [74]. To save time and cost, the long-branched OD side chain and TIPS groups were substituted by methyl and trimethylsilylethynyl, and the corresponding polymer backbones were simplified into oligomers with one repeating units (unimer), prior to the calculations. As presented in Figure 6, the HOMO orbitals are delocalized across the whole conjugated main chain, whereas, the LUMO orbitals are preferentially concentrated in the corresponding electron-deficient segments. These DFT calculations implied that the effective charge-transfer process would occur between the DTBDT-TIPS and BT/FBT/NT units. Accordingly, the calculated E_{HOMO}, E_{LUMO}, and bandgap were −4.97, −2.68, and 2.29 eV for PDTBDT-TIPS-DTBT-OD; −5.04, −2.78, and 2.26 eV for PDTBDT-TIPS-DTFBT-OD; and −5.01, −2.94, and 2.07 eV for PDTDBT-TIPS-DTNT-OD, respectively. Clearly, the variation trend of the E_{HOMO} was deepened by the fluorination and replacement of the BT with NT, agreeing well with results from the previous CV measurements. Moreover, it has already been demonstrated that good planarity of the polymer backbone is conducive to ensuring closer π–π stacking, which is propitious to internal aggregation, charge transfer, and molecular conjugation to engender a lower band gap [2]. Consequently, the dihedral angles θ_1 between the donor DTBDT-TIPS unit and the alkylthiophene bridge, θ_2, and θ_3, between the alkylthiophene bridge and the acceptor BT/FBT/NT moiety were 21.79°, −7.24°, and −4.10° for the DTBDT-TIPS-DTBT-OD; 22.29°, −1.06°, and −0.17° for the DTBDT-TIPS-DTFBT-OD; and 15.65°, −8.78°, and 2.96° for the DTBDT-TIPS-DTNT-OD, respectively, as shown in Figure S13. The molecular planarity was improved by both the fluorination and replacement of BT with NT, in good accordance with the previous XRD analyses and TD-Abs measurements. Interesting to note that the calculated data

were all higher in energy than those from the experimental test, since in the calculation process only the finite unimer and the short side chain were considered in the DFT model to describe the conjugated polymers. Notwithstanding, these theoretical calculation values agreed with the trends observed in the experiment and still disclosed the interrelation amongst the molecular structure, optoelectrical property, and thus the PV performance.

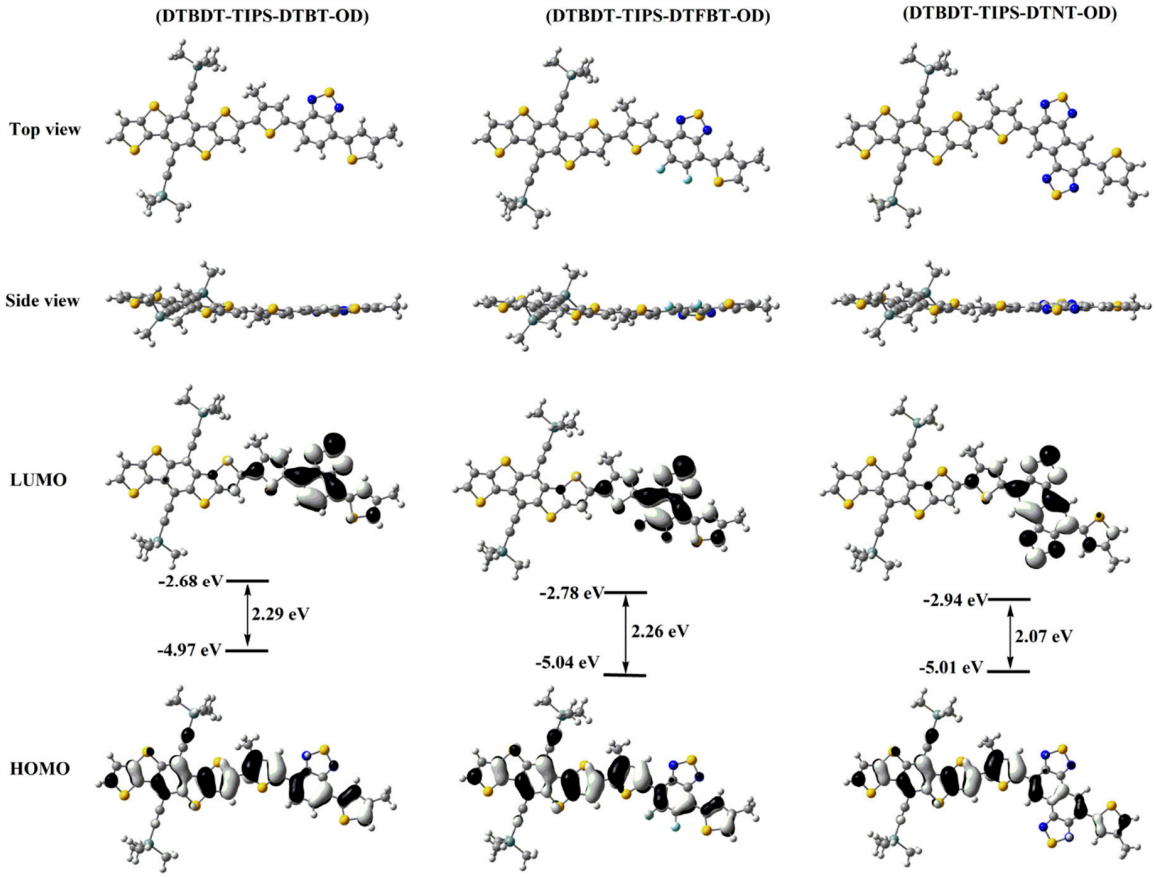

Figure 6. Caption optimized geometries and molecular orbital surfaces of the HOMO and LUMO for the unimer model compound of the DTBDT-TIPS-based polymers.

3.6. Photovoltaic Properties

To investigate the PV properties of these copolymers as donor materials in BHJ PSCs, the inverted devices evoked significantly the enhanced device stability where a structure of the ITO/PFN/polymers:PCBM/MoO_3/Ag was fabricated. Here, the active layers consisted of copolymers, and $PC_{61}BM$ or $PC_{71}BM$ were spin-coated from the CB solution, whilst a 10 nm thick PFN and an 8 nm thick MoO_3 were utilized as the cathode and anode interlayer, respectively, as described in References [75,76]. The performance was optimized using various processing parameters, including the D/A blend ratio, the usage of processing additive, and the replacement of $PC_{61}BM$ with $PC_{71}BM$. The detailed device fabrication process is presented in the supporting Information (Figures S14, S15 and Table S3). *J*–*V* characteristics were characterized under AM 1.5G illumination at 100 mW cm^{-2} using a solar simulator. Firstly, it is widely recognized that the donor polymer/$PC_{61}BM$ (D/A) weight ratio plays a significant and vital role in improving the PV performance of the corresponding devices [49,77,78]. Consequently, the devices from each of the polymer weight ratios of the D/A ratios, such as 1:1, 1:1.5, to 1:2 were fabricated, and it was found that the best D/A ratio for all the copolymers was 1:1.5 in Figure S14, and the detailed parameters are summarized in Table S3. The PDTBDT-TIPS-DTBT-OD-based device showed the best PCE of 1.37%, with a V_{OC} of 0.91 V, a J_{SC} of 3.32 mA cm^{-2}, and a *FF* of 45.21%. The fluorinated PDTBDT-TIPS-DTFBT-OD exhibited an inferior

PCE of 1.09%, with a lower J_{SC} of 2.19 mA cm^{-2}, even with an increased V_{OC} of 0.93 V, and *FF* of 53.59%. The PDTBDT-TIPS-DTNT-OD-based device also showed an inferior PCE of 1.15%, with a simultaneous decreased V_{OC} of 0.88 V, a J_{SC} of 3.19 mA cm^{-2}, and a *FF* of 40.55%. Obviously, the EQE curves in Figure S14 validated the variations of the J_{SC} in *J*–*V* measurement.

Plenty of researches have demonstrated that the solvent additive 1,8-diiodoctane (DIO) can help active layers to form a more ordered and nanoscale bicontinuous interpenetration network, which facilitates efficient charge generation and transport, and hence improves the PV performance of the corresponding devices [79,80]. Subsequently, the 3% DIO (DIO/CB, V/V) was selected as a solvent additive during the device fabrication and the *J*–*V* curves are shown in Figure S15. A significant 163% enhancement in the PCE (from 1.15% to 3.03%) in the PDTBDT-TIPS-DTNT-OD-based device was achieved, which benefited from a large 120% enhancement in the J_{SC} (from 3.19 to 7.03 mA cm^{-2}) and a 21.8% increase in the *FF* (from 40.55% to 49.39%), even though the V_{OC} remained stable. For the control PDTBDT-TIPS-DTBT-OD-based device, it exhibited a slightly inferior PCE of 1.03%, influenced by a decline of 43% in the J_{SC} (from 3.32 to 1.89 mA cm^{-2}). Unfortunately, the fluorinated PDTBDT-TIPS-DTFBT-based device showed a 59.6% drop in the PCE (from 1.09% to 0.44%), which was ascribed to simultaneous 3.2%, 53.0%, and 26.1% declines in the V_{OC}, J_{SC}, and *FF* (from 0.93 to 0.90 V, from 2.19 to 1.03 mA cm^{-2}, and from 53.59% to 39.58%), respectively. Evidently, the DIO may play a positive role in the PDTBDT-TIPS-DTNT-OD-based cell; however, it gives rise to an adverse effect in the PDTBDT-TIPS-DTBT-OD- and PDTBDT-TIPS-DTFBT-OD-based devices.

Owing to $PC_{71}BM$ bearing similar electronic properties to $PC_{61}BM$, but with a considerably higher absorption coefficient and a broader absorption spectrum, $PC_{71}BM$ was further applied instead of $PC_{61}BM$ to maximize the PCE [81]. As seen in Figure S13 and Table S3, the PCE of the PDTBDT-TIPS- DTBT-OD based device slightly increased by approximately 7.3% (from 1.37% to 1.47%), which originated from a 9.0% enhancement in the J_{SC} (from 3.32 to 3.62 mA cm^{-2}) and the *FF* (from 45.21% to 50.93%), but with a decreased V_{OC} (from 0.91 V to 0.80 V). Regrettably, an improvement in the PCE for the fluorinated system was not observed. However, as for the PDTBDT-TIPS-DTFBT-OD-based device, an 11.2% enhancement in the PCE (from 3.03% to 3.37%) was observed, and this improvement was ascribed to the 2.56% (from 7.03 to 7.21 mA cm^{-2}) and 3.60% (from 49.39% to 52.99%) increases in the corresponding J_{SC} and *FF*, whilst the V_{OC} remained stable. Evidently, these variations agreed well with the corresponding EQE curves in Figure S15, in particular, there existed a distinct improvement ranging from 400 to 550 nm in the EQE profile related to the contribution of the $PC_{71}BM$.

Going through the previous series of device fabrication optimization, including the D/A ratio, the DIO additive, and the replacement of $PC_{61}BM$ with $PC_{71}BM$, the best *J*–*V* curves and EQE spectra of the studied polymers are shown in Figure 7, and the best PV data are listed in Table 2. Owing to incorporation of the DTBDT-TIPS into the polymer backbones as D units, the polymers containing the TIPS PV devices all had a higher V_{OC} in the range of 0.80–0.93 V, and the V_{OC} values increased after fluorination and the replacement of the BT with NT, in agreement with the predictions of a previous deeper E_{HOMO} in the DFT calculation and CV measurement [4]. It was exhibited that the optimal PCE decreased from 1.47% to 1.09% with the incorporation of fluorine into BT, which was ascribed to the 39.5% reduction in the J_{SC} (from 3.62 to 2.19 mA cm^{-2}), despite a 16.25% increase in the V_{OC} (from 0.80 to 0.93 V) and a 5.16% increase in the *FF* (from 50.96% to 53.59%). Interestingly, when replacing the BT with NT, a 129% enhancement in the PCE (from 1.47% to 3.37%) was realized, which benefited from 10% (from 0.80 V to 0.88 V), 99.2% (from 3.62 to 7.21 mA cm^{-2}), and 3.98% (from 50.96% to 52.99%) increases in the corresponding V_{OC}, J_{SC}, and *FF* of the devices. From Figure 7b, photo-response profiles of the optimal devices in the ranges of 300–720 nm for the PDTBDT-TIPS-DTBT-OD, 300–680 nm for the PDTBDT-TIPS-DTFBT-OD, and 300–760 nm for the PDTBDT-TIPS-DTNT-OD, were observed. The higher J_{SC} in the PDTBDT-TIPS-DTNT-OD-based device was due to its broadened absorption and higher EQE value. Moreover, the integrated J_{SC} values from the EQE curves were 3.50, 2.08, and 7.09 mA cm^{-2}, for the best-performing PDTBDT-TIPS-DTBT-HD:$PC_{71}BM$,

PDTBDT-TIPS-DTFBT-HD:$PC_{61}BM$, and PBDT-TIPS-DTNT-OD:$PC_{71}BM$, respectively, which was indicative of an error smaller than 5% compared to the J_{SC} value obtained from the *J*–*V* curves.

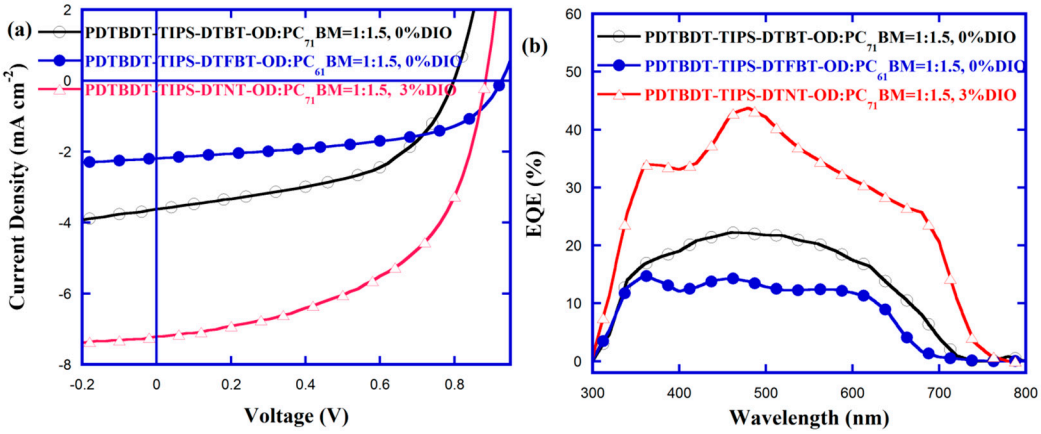

Figure 7. The optimized current density–voltage (*J*–*V*) curves (**a**) and external quantum efficiency (EQE) spectra (**b**) of the optimized devices.

Table 2. The optimized photovoltaic (PV) parameters of polymer solar cells (PSCs) based on the studied copolymers.

Active Layer	Ratio/ Additive	V_{OC} (V)	J_{SC} (mA cm^{-2}) [a]	*FF* (%)	PCE (%)
PDTBDT-TIPS-DTBT-OD/$PC_{71}BM$	1:1.5/0%DIO	0.80	3.62 (3.50)	50.96	1.47
PDTBDT-TIPS-DTFBT-OD/$PC_{61}BM$	1:1.5/0%DIO	0.93	2.19 (2.08)	53.59	1.09
PDTBDT-TIPS-DTNT-OD/$PC_{71}BM$	1:1.5/3%DIO	0.88	7.21 (7.09)	52.99	3.37

[a] The values in the parentheses are the integrated currents obtained from the EQE curves.

3.7. Charge Mobilities

To find the reason for the different photovoltaic performance on fluorination and on replacement of the BT with NT on the polymer backbone, the vertical hole transport property was examined and hole-only devices of polymer:PCBM blend films were fabricated under identical conditions to the optimized PSCs. The hole mobilities estimated using the SCLC method could be described by the equation $J = \frac{9}{8}\varepsilon_0\varepsilon_r\mu_h\frac{V^2}{L^3}$ as described in References [66,82]. Worth noting that the thickness was 87 nm for the PDTBDT-TIPS-DTBT-OD, 80 nm for the PDTBDT-TIPS-DTFBT-OD, and 127 nm for the PDTBDT-TIPS- DTNT-OD, respectively. As shown in Figure 8, the $J^{1/2}$–*V* curves of the active layers were obtained in the dark for the hole-only devices. The perfect linear fitting in the figure indicates that the $J^{1/2}$–*V* follow the Mott-Gurney square law. Accordingly, the μ_hs of the PDTBDT-TIPS-DTBT-OD, PDTBDT-TIPS- DTFBT-OD, and PDTBDT-TIPS-DTNT-OD were calculated to be 2.32×10^{-5}, 3.98×10^{-5}, and 9.09×10^{-5} cm^2 V^{-1} s^{-1}, respectively, (Table S4). Apparently, such variation tendencies in mobility was consistent with the results of the XRD and DFT calculations. The highest SCLC hole mobility could partially account for the observed markedly higher J_{SC} in the PDTBDT-TIPS-DTNT-OD-based cell.

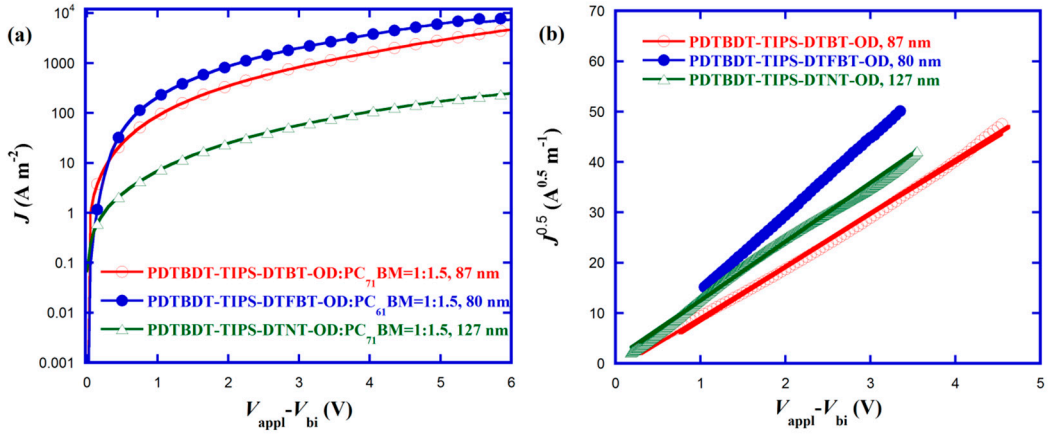

Figure 8. J–V (**a**) and $J^{1/2}$–V (**b**) characteristics of the hole-only devices.

3.8. Film Morphology

As is known, performances of BHJ PSCs are strongly associated with the morphologies of the active layer [79,83]. Therefore, to understand the reasons why the fluorination and the NT substitution of BT had such different photovoltaic performances, the morphologies of the optimized blend films were investigated using tapping-model atomic force microscopy (AFM) on a surface area of 5 × 5 μm^2. The AFM topography and the phase images of the three copolymers showed the different morphologies. As shown in Figure 9, the blend film of the PDTBDT-TIPS-DTBT-OD:$PC_{71}BM$ with 3% DIO had a very smooth surface with a root-mean-square (RMS) roughness of only 0.478 nm, but with an inconspicuous phase separation. For the blend film of the fluorinated PDTBDT-TIPS-DTFBT-OD:$PC_{61}BM$ without DIO, it exhibited a very rough surface with an RMS of 10.62 nm and oversized aggregation, which severely limits the effective exciton diffusion and deteriorates the exciton dissociation probability by reducing the D/A interfacial areas, resulting in a poor J_{SC} [83]. Worth noting that the blend film of PDTBDT-TIPS-DTNT-OD:$PC_{71}BM$ with 3% DIO had an appropriate surface with an RMS roughness of 5.202 nm and a proper phase separation, forming a bicontinuous interpenetrating network structure, which could support the D/A interfacial areas to promote the exciton dissociation into the free charges, but it also assisted the free charges to transport to the corresponding electrodes [4]. To further inspect the composition and in-depth morphology of the active layers, transmission electron microscopy (TEM) was applied. As is known, owing to the big difference in electron scattering density between polymers (1.1 g cm^{-3}) and fullerene derivatives (1.5 g cm^{-3}), the polymer networks and porous regions are imaged as lighter (copolymer) and darker ($PC_{71}BM$) colored in the TEM, respectively [65]. As depicted in Figure 10, it was found that after incorporating F into BT, there was oversized polymer aggregation. Meanwhile, the improved phase separation and partial fibril nanostructure were observed when substituting the BT with NT, similar to the results observed in former AFM. Therefore, the morphological information could partially explain that the fluorination led to a decreased J_{SC}, whereas the replacement of the BT with NT resulted in a significantly increased J_{SC} and slightly improved *FF*.

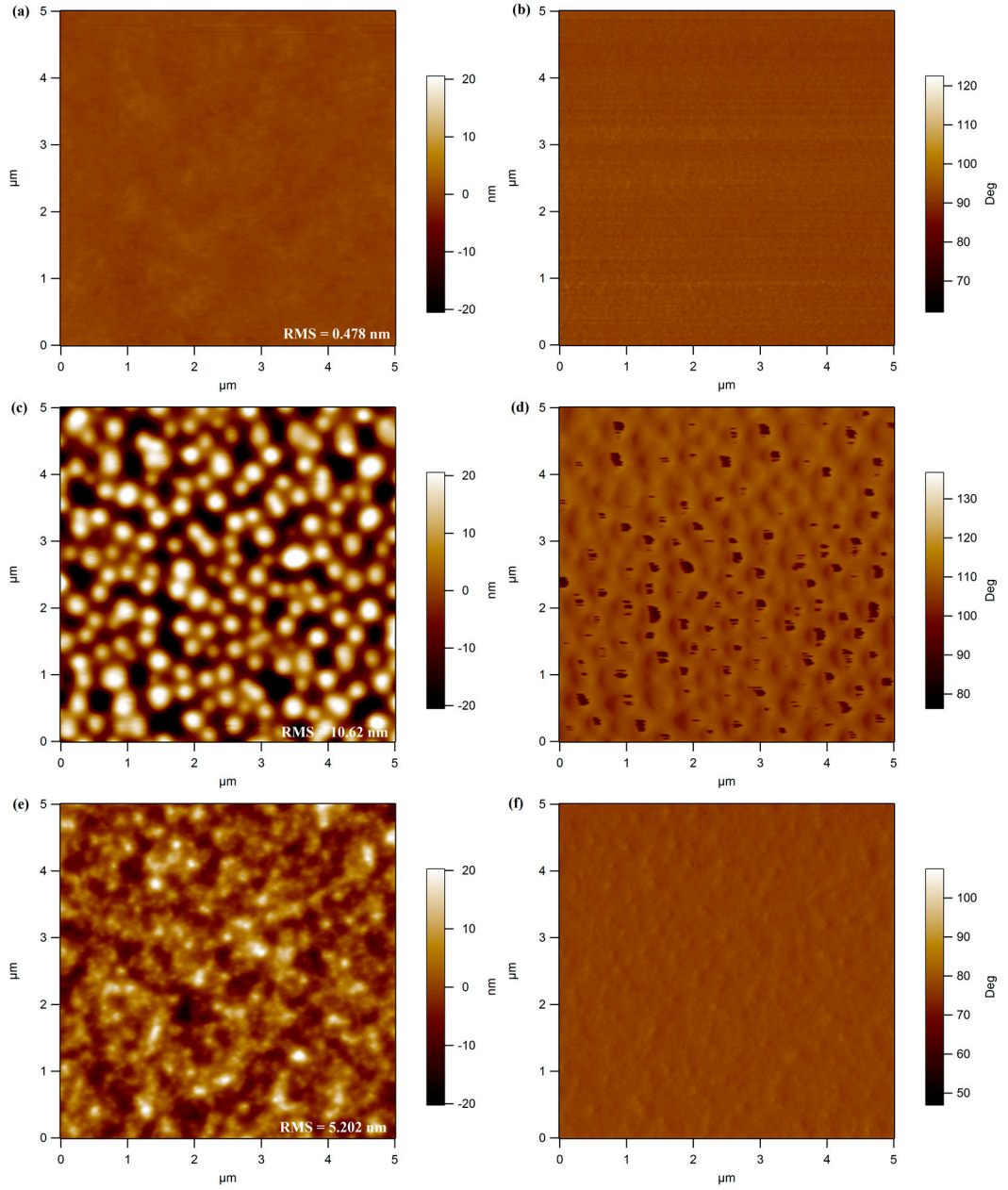

Figure 9. Tapping Atomic force microscopy (AFM) height (**left**) and phase (**right**) images of the active layers of PDTBDT-TIPS-DTBT-OD/$PC_{71}BM$ (1:1.5, 0%DIO, **a**,**b**), PDTBDT-TIPS-DTFBT-OD/$PC_{61}BM$ (1:1.5, 0%DIO, **c**,**d**) and PDTBDT-TIPS-DTNT-OD/$PC_{71}BM$ (1:1.5, 3%DIO, **e**,**f**). Image size: 5 µm × 5 µm.

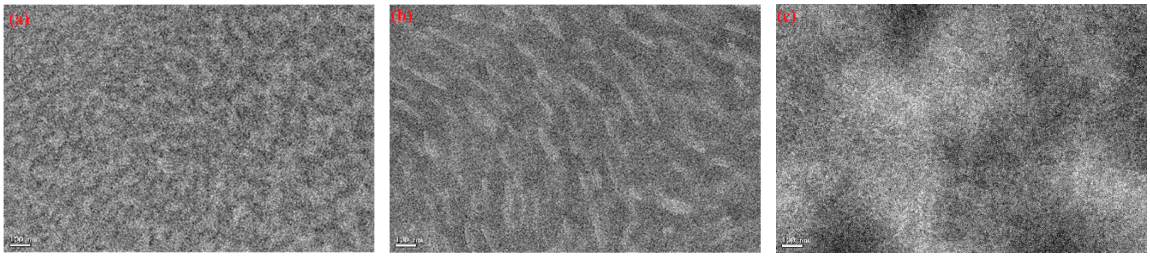

Figure 10. Transmission electron microscopy (TEM) bright field images of active layers for PDTBDT-TIPS-DTBT-OD/$PC_{71}BM$ (1:1.5, 0%DIO, **a**), PDTBDT-TIPS-DTFBT-OD/$PC_{61}BM$ (1:1.5, 0%DIO, **b**) and PDTBDT-TIPS-DTNT-OD/$PC_{71}BM$ (1:1.5, 3%DIO, **c**).

4. Conclusions

To sum up, three alternated D-π-A type CPs, PDTBDT-TIPS-DTBT-OD, PDTBDT-TIPS- DTFBT-OD, and PDTBDT-TIPS-DTNT-OD, in which A units were varied among BT, FBT, and NT, were designed and prepared. By changing the A moieties of the D-π-A polymer backbone, E_g^{opt}, E_{HOMO} and E_{LUMO} could be validly tuned and varied in the ranges of 1.83~1.67 eV, −5.35~−5.46 eV, and −3.46~−3.66 eV, respectively. It was exhibited that the absorption profile was scarcely influenced by the fluorination on BT; however, it was greatly broadened after replacing the BT with NT. The E_{HOMO}s were effectively deepened and the intermolecular aggregation in the CB solution and solid film state were improved. The optimal photovoltaic measurements demonstrated that replacing the BT with NT in PDTBDT-TIPS-DTNT-OD exhibited a simultaneous elevated V_{OC} of 0.88 V, J_{SC} of 7.21 mA cm^{-2}, and *FF* of 52.99%, and resulted in a PCE of 3.37%, which was 1.29 times higher relative to its counterpart. These improvements originated from the greatly broadened absorption, lower E_{HOMO}, improved molecular ordered structure, and the enhanced SCLC mobility and favorable morphology of the active layer. However, the PCE decreased by 25.9% from fluorination because of the suppressed J_{SC}, resulting in an unfavorable blend film morphology despite a high V_{OC}. Our preliminary results suggested that replacing the BT with NT in the D-π-A type polymer backbone was an effective method aimed at highly efficient PSCs.

Supplementary Materials: Detailed experimental procedures and additional characterization data are available online at http://www.mdpi.com/2073-4360/11/1/12/s1. Scheme S1, Synthesis of dibromide DTBT-ODBr$_2$ and DTFBT-ODBr$_2$; Scheme S2, Synthesis of bistin comonomer DTBDT-TIPSSn; Figure S1 ^{1}H NMR spectrum of DTBT-OD in $CDCl_3$; Figure S2 ^{1}H NMR spectrum of DTBT-ODBr$_2$ in $CDCl_3$; Figure S3 ^{1}H NMR spectrum of DTFBT-OD in $CDCl_3$; Figure S4 ^{1}H NMR spectrum of DTFBT-ODBr$_2$ in $CDCl_3$; Figure S5 ^{1}H NMR spectrum of DTBDT-TIPS in $CDCl_3$; Figure S6 ^{1}H NMR spectrum of DTBDT-TIPSSn in $CDCl_3$; Figure S7 ^{1}H NMR spectrum of PDTBDT-TIPS-DTBT-OD in $CDCl_3$; Figure S8 ^{1}H NMR spectrum of PDTBDT-TIPS-DTFBT-OD in $CDCl_3$; Figure S9 ^{1}H NMR spectrum of PDTBDT-TIPS-DTNT-OD in $CDCl_3$; Figure S10 The TGA curves of copolymers containing DTBDT-TIPS; Figure S11 UV-vis absorption spectra of DTBDT-TIPS-based copolymers dissolved in CB at various concentrations and calculation of molar absorption coefficient; Figure S12 UV-vis absorption spectra of DTBDT-TIPS-based copolymers in film at varied thickness and calculation of molar absorption coefficient; Figure S13 Dihedral angles for the unimer model compound of copolymers; Figure S14 The *J*–*V* curves of DTBDT-TIPS-based polymers with different D/A weight ratios to $PC_{61}BM$ and EQE spectra of corresponding PSCs; Figure S15 The *J*–*V* curves of polymers without and with 3%DIO, $PC_{61}BM$ replacing with $PC_{71}BM$ and EQE spectra of corresponding PSCs; Table S1 Yields, GPC data, thermal properties for DTBDT-TIPS-based polymers; Table S2 Absorption coefficients for copolymers; Table S3. The photovoltaic performance of the PSCs devices with different blend ratio, without/with 3% (volume) DIO, and using $PC_{71}BM$ replacing of $PC_{61}BM$; Table S4 Hole mobilities of polymers and blend measured by SCLC model.

Author Contributions: J.T. wrote the paper, designed the experiments, analyzed the data, and discussed the results. L.A. and P.G. prepared the conjugated polymers. J.L., and C.Y. contributed to the measurements of the solar cells and corresponding analysis. X.W. finished the DFT calculations. Y.X. revised the manuscript. All authors read and approved the final manuscript.

Funding: The authors are deeply grateful to the National Nature Science Foundation of China (51463011, 51602139, 21805122 and 61404067), the Natural Science Foundation of Gansu Province, (Grant No.: 18JR3RA108), the Foundation of A Hundred Youth Talents Training (152022), and the Excellent Team of Scientific Research in Lanzhou Jiaotong University (201705, 201703) for financial support.

Acknowledgments: The authors are deeply grateful to the National Nature Science Foundation of China (51463011, 51602139, 21805122 and 61404067), the Natural Science Foundation of Gansu Province, (Grant No.: 18JR3RA108), the Foundation of A Hundred Youth Talents Training (152022), and the Excellent Team of Scientific Research in Lanzhou Jiaotong University (201705, 201703) for financial support. We also express our thanks to the Instrument Analysis Center of Lanzhou Jiaotong University for related testing support.

Conflicts of Interest: The authors declare no conflict of interest.

References

1. Cheng, P.; Zhan, X. Stability of organic solar cells: Challenges and strategies. *Chem. Soc. Rev.* **2016**, *45*, 2544–2582. [CrossRef] [PubMed]
2. Qin, Y.; Liu, S.; Gu, H.; Dai, W.; Luo, X. Highly flattened donor-acceptor polymers based on fluoride-substituent acceptors for efficient heterojunction solar cells. *Sol. Energy* **2018**, *166*, 450–457. [CrossRef]
3. Li, G.; Zhu, R.; Yang, Y. Polymer solar cells. *Nat. Photonics* **2012**, *6*, 153–161. [CrossRef]
4. Li, Y. Molecular design of photovoltaic materials for polymer solar cells: Toward suitable electronic energy levels and broad absorption. *Acc. Chem. Res.* **2012**, *45*, 723–733. [CrossRef] [PubMed]
5. Liu, Y.; Zhao, J.; Li, Z.; Mu, C.; Ma, W.; Hu, H.; Jiang, K.; Lin, H.; Ade, H.; Yan, H. Aggregation and morphology control enables multiple cases of high-efficiency polymer solar cells. *Nat. Commun.* **2014**, *5*, 5293. [CrossRef] [PubMed]
6. Zhao, J.; Li, Y.; Yang, G.; Jiang, K.; Lin, H.; Ade, H.; Ma, W.; Yan, H. Efficient organic solar cells processed from hydrocarbon solvents. *Nat. Energy* **2016**, *1*, 15027. [CrossRef]
7. Jin, Y.; Chen, Z.; Xiao, M.; Peng, J.; Fan, B.; Ying, L.; Zhang, G.; Jiang, X.-F.; Yin, Q.; Liang, Z.; et al. Thick film polymer solar cells based on naphtho[1,2-*c*:5,6-*c*′]bis[1,2,5]thiadiazole conjugated polymers with efficiency over 11%. *Adv. Energy Mater.* **2017**, *7*, 1700944. [CrossRef]
8. Zhao, W.; Li, S.; Yao, H.; Zhang, S.; Zhang, Y.; Yang, B.; Hou, J. Molecular optimization enables over 13% efficiency in organic solar cells. *J. Am. Chem. Soc.* **2017**, *139*, 7148–7151. [CrossRef]
9. Bundgaard, E.; Krebs, F.C. Low band gap polymers for organic photovoltaics. *Sol. Energy Mater. Sol. Cells* **2007**, *91*, 954–985. [CrossRef]
10. Zhou, H.; Yang, L.; You, W. Rational design of high performance conjugated polymers for organic solar cells. *Macromolecules* **2012**, *45*, 607–632. [CrossRef]
11. Xu, T.; Yu, L. How to design low bandgap polymers for highly efficient organic solar cells. *Mater. Today* **2014**, *17*, 11–15. [CrossRef]
12. Qi, B.; Wang, J. Open-circuit voltage in organic solar cells. *J. Mater. Chem.* **2012**, *22*, 24315–24325. [CrossRef]
13. Elumalai, N.K.; Uddin, A. Open circuit voltage of organic solar cells: An in-depth review. *Energy Environ. Sci.* **2016**, *9*, 391–410. [CrossRef]
14. Chen, Z.; Cai, P.; Chen, J.; Liu, X.; Zhang, L.; Lan, L.; Peng, J.; Ma, Y.; Cao, Y. Low band-gap conjugated polymers with strong interchain aggregation and very high hole mobility towards highly efficient thick-film polymer solar cells. *Adv. Mater.* **2014**, *26*, 2586–2591. [CrossRef] [PubMed]
15. Ma, Y.; Chen, H.; Tang, Y.; Wang, J.-Y.; Ma, W.; Zheng, Q. Modulation of bulk heterojunction morphology through small π-bridge changes for polymer solar cells with enhanced performance. *J. Mater. Chem. C* **2018**, *6*, 5999–6007. [CrossRef]
16. Zhang, Z.-G.; Wang, J. Structures and properties of conjugated Donor-Acceptor copolymers for solar cell applications. *J. Mater. Chem.* **2012**, *22*, 4178–4187. [CrossRef]
17. Kim, H.G.; Jo, S.B.; Shim, C.; Lee, J.; Shin, J.; Cho, E.C.; Ihn, S.-G.; Choi, Y.S.; Kim, Y.; Cho, K. Synthesis and photovoltaic properties of benzo[1,2-*b*:4,5-*b*′]dithiophene derivative-based polymers with deep HOMO levels. *J. Mater. Chem.* **2012**, *22*, 17709–17717. [CrossRef]
18. Hou, J.; Park, M.-H.; Zhang, S.; Yao, Y.; Chen, L.-M.; Li, J.-H.; Yang, Y. Bandgap and molecular energy level control of conjugated polymer photovoltaic materials based on benzo[1,2-*b*:4,5-*b*′]dithiophene. *Maromolecules* **2008**, *41*, 6012–6601. [CrossRef]
19. Du, J.; Biewer, M.C.; Stefan, M.C. Benzothiadiazole building units in solution-processable small molecules for organic photovoltaics. *J. Mater. Chem. A* **2016**, *4*, 15771–15787. [CrossRef]
20. Wang, Y.; Michinobu, T. Benzothiadiazole and its π-extended, heteroannulated derivatives: Useful acceptor building blocks for high-performance donor-acceptor polymers in organic electronics. *J. Mater. Chem. C* **2016**, *4*, 6200–6214. [CrossRef]
21. Mori, H.; Nishinaga, S.; Takahashi, R.; Nishihara, Y. Alkoxy-substituted anthra[1,2-c:5,6-c′]bis([1,2,5]-thiadiazole) (ATz): A new electron-acceptor unit in the semiconducting polymers for organic electronics. *Macromolecules* **2018**, *51*, 5473–5484. [CrossRef]
22. Blouin, N.; Michaud, A.; Leclerc, M. A low-bandgap poly(2,7-carbazole) derivative for use in high-performance solar cells. *Adv. Mater.* **2007**, *19*, 2295–2300. [CrossRef]

23. Peet, J.; Kim, J.Y.; Coates, N.E.; Ma, W.L.; Moses, D.; Heeger, A.J.; Bazan, G.C. Efficiency enhancement in low-bandgap polymer solar cells by processing with alkane dithiols. *Nat. Mater.* **2007**, *6*, 497–500. [CrossRef]
24. Osaka, I.; Shimawaki, M.; Mori, H.; Doi, I.; Miyazaki, E.; Koganezawa, T.; Takimiya, K. Synthesis, characterization, and transistor and solar cell applications of a naphthobisthiadiazole-based semi-conducting polymer. *J. Am. Chem. Soc.* **2012**, *134*, 3498–3507. [CrossRef] [PubMed]
25. Wang, M.; Hu, X.; Liu, P.; Li, W.; Gong, X.; Huang, F.; Cao, Y. Donor-acceptor conjugated polymer based on naphtho[1,2-*c*:5,6-*c*′]bis[1,2,5]thiadiazole for high-performance polymer solar cells. *J. Am. Chem. Soc.* **2011**, *133*, 9638–9641. [CrossRef] [PubMed]
26. Guo, P.; Xia, Y.; Huang, F.; Luo, G.; Li, J.; Zhang, P.; Zhu, Y.; Yang, C.; Wu, H.; Cao, Y. An alkylthieno-2-yl flanked dithieno[2,3-*d*:2′,3′-*d*′]benzo[1,2-*b*:4,5-*b*′]dithiophene-based low band gap conjugated polymer for high performance photovoltaic solar cells. *RSC Adv.* **2015**, *5*, 12879–12885. [CrossRef]
27. Zhou, H.; Yang, L.; Stuart, A.C.; Price, S.C.; Liu, S.; You, W. Development of fluorinated benzothiadi-azole as a structural unit for a polymer solar cell of 7% efficiency. *Angew. Chem.* **2011**, *123*, 3051–3054. [CrossRef]
28. Jo, J.W.; Jung, J.W.; Wang, H.-W.; Kim, P.; Russell, T.P.; Jo, W.H. Fluorination of polythiophene derivatives for high performance organic photovoltaics. *Chem. Mater.* **2014**, *26*, 4214–4220. [CrossRef]
29. Li, Z.; Lin, H.; Jiang, K.; Carpenter, J.; Li, Y.; Liu, Y.; Hu, H.; Zhao, J.; Ma, W.; Ade, H.; et al. Dramatic performance enhancement for large bandgap thick-film polymer solar cells introduced by a difluorinated donor unit. *Nano Energy* **2015**, *15*, 607–615. [CrossRef]
30. Wolf, J.; Cruciani, F.; El Labban, A.; Beaujuge, P.M. Wide band-gap 3,4-difluorothiophene-based polymer with 7% solar cell efficiency: An alternative to P3HT. *Chem. Mater.* **2015**, *27*, 4184–4187. [CrossRef]
31. Hu, H.; Jiang, K.; Kim, J.-H.; Yang, G.; Li, Z.; Ma, T.; Lu, G.; Qu, Y.; Ade, H.; Yan, H. Influence of fluorination on the properties and performance of isoindigo-quaterthiophene-based polymers. *J. Mater. Chem. A* **2016**, *4*, 5039–5043. [CrossRef]
32. Leclerc, N.; Chávez, P.; Ibraikulov, O.A.; Heiser, T.; Lévêque, P. Impact of backbone fluorination on π-conjugated polymers in organic photovoltaic devices: A review. *Polymers* **2016**, *8*, 11. [CrossRef]
33. Lee, H.S.; Song, H.G.; Jung, H.; Kim, M.H.; Cho, C.; Lee, J.-Y.; Park, S.; Son, H.J.; Yun, H.-J.; Kwon, S.-K.; et al. Effects of backbone planarity and tightly packed alkyl chains in the donor-acceptor polymers for high photostability. *Macromolecules* **2016**, *49*, 7844–7856. [CrossRef]
34. Xu, X.-P.; Li, Y.; Luo, M.-M.; Peng, Q. Recent progress towards fluorinated copolymers for efficient photovoltaic applications. *Chin. Chem. Lett.* **2016**, *27*, 1241–1249. [CrossRef]
35. Zhang, S.; Qin, Y.; Uddin, M.A.; Jang, B.; Zhao, W.; Liu, D.; Woo, H.Y. Hou, J. A fluorinated polythiophene derivative with stabilized backbone conformation for highly efficient fullerene and non-fullerene polymer solar cells. *Macromolecules* **2016**, *49*, 2993–3000. [CrossRef]
36. Wang, T.; Lau, T.-K.; Lu, X.; Yuan, J.; Feng, L.; Jiang, L.; Deng, W.; Peng, H.; Li, Y.; Zou, Y. A medium bandgap D-A copolymer based on 4-alkyl-3,5-difluorophenyl substituted quinoxaline unit for high performance solar cells. *Macromolecules* **2018**, *51*, 2838–2846. [CrossRef]
37. Zhang, Y.; Chien, S.-C.; Chen, K.-S.; Yip, H.-L.; Sun, Y.; Davies, J.A.; Chen, F.-C.; Jen, A.K.-Y. Increased open circuit voltage in fluorinated benzothiadiazole-based alternating conjugated polymers. *Chem. Commun.* **2011**, *47*, 11026–11028. [CrossRef]
38. Min, J.; Zhang, Z.-G.; Zhang, S.; Li, Y. Conjugated side-chain-isolated D-A copolymers based on benzo[1,2-*b*:4,5-*b*′]dithiophene-*alt*-dithienylbenzotriazole: Synthesis and photovoltaic properties. *Chem. Mater.* **2012**, *24*, 3247–3254. [CrossRef]
39. Stuart, A.C.; Tumbleston, J.R.; Zhou, H.; Li, W.; Liu, S.; Ade, H.; You, W. Fluorine substituents reduce charge recombination and drive structure and morphology development in polymer solar cells. *J. Am. Chem. Soc.* **2013**, *135*, 1806–1815. [CrossRef] [PubMed]
40. Kawashima, K.; Fukuhara, T.; Suda, Y.; Suzuki, Y.; Koganezawa, T.; Yoshida, H.; Ohkita, H.; Osaka, I.; Takimiya, K. Implication of fluorine atom on electronic properties, ordering structures, and photovoltaic performance in naphthobisthiadiazole-based semiconducting polymers. *J. Am. Chem. Soc.* **2016**, *138*, 10265–10275. [CrossRef]
41. Price, S.C.; Stuart, A.C.; Yang, L.; Zhou, H.; You, W. Fluorine substituted conjugated polymer of medium band gap yields 7% efficiency in polymer-fullerene solar cells. *J. Am. Chem. Soc.* **2011**, *133*, 4625–4631. [CrossRef] [PubMed]

42. Li, Z.; Lu, J.; Tse, S.-C.; Zhou, J.; Du, X.; Tao, Y.; Ding, J. Synthesis and applications of difluorobenzo-thiadiazole based conjugated polymers for organic photovoltaics. *J. Mater. Chem.* **2012**, *21*, 3226–3233. [CrossRef]
43. Jo, J.W.; Bae, S.; Liu, F.; Russell, T.P.; Jo, W.H. Comparison of two D-A type polymers with each being fluorinated on D and A unit for high performance solar cells. *Adv. Funct. Mater.* **2015**, *2*, 120–125. [CrossRef]
44. Zhang, Y.; Zou, J.; Cheuh, C.-C.; Yip, H.-L.; Jen, A.K.-Y. Significant improved performance of photovoltaic cells made from a partially fluorinated cyclopentadithiophene/benzothiadiazole conjugated polymer. *Macromolecules* **2012**, *45*, 5427–5435. [CrossRef]
45. Iyer, A.; Bjorgaard, J.; Anderson, T.; Köse, M.E. Quinoxaline-based semiconducting polymers: Effect of fluorination on the photophysical, thermal, and charge transport properties. *Macromolecules* **2012**, *45*, 6380–6389. [CrossRef]
46. Schroeder, B.C.; Huang, Z.; Ashraf, R.S.; Smith, J.; D'Angelo, P.; Watkins, S.E.; Anthopoulos, T.D.; Durrant, J.R.; McCulloch, I. Silaindacenodithiophene-based low band gap polymers-the effect of fluorine substitution on device performances and film morphologies. *Adv. Funct. Mater.* **2012**, *22*, 1663–1670. [CrossRef]
47. Jin, Y.; Chen, Z.; Dong, S.; Zheng, N.; Ying, L.; Jiang, X.-F.; Liu, F.; Huang, F.; Cao, Y. A novel naphtho[1,2-*c*:5,6-*c*′]bis([1,2,5]thiadiazole)-based narrow-bandgap π-conjugated polymer with power conversion efficiency over 10%. *Adv. Mater.* **2016**, *28*, 9811–9818. [CrossRef]
48. Osaka, I.; Takimiya, K. Naphthobischalcogenadiazole conjugated polymers: Emerging materials for organic electronics. *Adv. Mater.* **2017**, *29*, 1605218. [CrossRef]
49. Tong, J.; Li, J.; Zhang, P.; Ma, X.; Wang, M.; An, L.; Sun, J.; Guo, P.; Yang, C.; Xia, Y. Naphtho[1,2-*c*:5,6-*c*′]-bis[1,2,5]thiadiazole-based conjugated polymers consisting of oligothiophenes for efficient polymer solar cells. *Polymer* **2017**, *121*, 183–195. [CrossRef]
50. Xu, X.; Feng, K.; Li, K.; Peng, Q. Synthesis and photovoltaic properties of two dimensional benzodithiophene-thiophene copolymers with pendent rational naphtho[1,2-*c*:5,6-*c*]bis[1,2,5]thiadiazole side chains. *J. Mater. Chem. A* **2017**, *3*, 23149–23161. [CrossRef]
51. Shin, N.; Yun, H.-J.; Yoon, Y.; Son, H.J.; Ju, S.-Y.; Kwon, S.-K.; Kim, B.S.; Kim, Y.-H. Highly stable polymer solar cells based on poly(dithienobenzodithiophene-*co*-thienothiophene). *Macromolecules* **2015**, *48*, 3890–3899. [CrossRef]
52. Son, H.; Lu, L.; Chen, W.; Xu, T.; Zheng, T.; Carsten, B.; Strzalka, J.; Darling, S.; Chen, L.; Yu, L. Synthesis and photovoltaic effect in dithieno[2,3-*d*:2′,3′-*d*′]benzo[1,2-*b*:4,5-*b*′]dithiophene-based conjugated polymers. *Adv. Mater.* **2013**, *25*, 838–843. [CrossRef] [PubMed]
53. Wu, Y.; Li, Z.; Ma, W.; Huang, Y.; Huo, L.; Guo, X.; Zhang, M.; Ade, H.; Hou, J. PDT-S-T: A new polymer with optimized molecular conformation for controlled aggregation and π–π stacking and its application in efficient photovoltaic devices. *Adv. Mater.* **2013**, *25*, 3449–3455. [CrossRef] [PubMed]
54. Sun, S.; Zhang, P.; Li, J.; Li, Y.; Wang, J.; Zhang, S.; Xia, Y.; Meng, X.; Fan, D.; Chu, J. Synthetically controlling the optoelectronic properties of dithieno[2,3-*d*:2′,3′-*d*′]benzo[1,2-*b*:4,5-*b*′]dithiophene-*alt*-diketopyrrolopyrrole-conjugated polymers for efficient solar cells. *J. Mater. Chem. A* **2014**, *2*, 15316–15325. [CrossRef]
55. Huo, L.; Liu, T.; Sun, X.; Cai, Y.; Heeger, A.J.; Sun, Y. Single-junction organic solar cells based on a novel wide-bandgap polymer with efficiency of 9.7%. *Adv. Mater.* **2015**, *27*, 2938–2944. [CrossRef]
56. Zhong, W.; Xiao, J.; Sun, S.; Jiang, X.-F.; Lan, L.; Ying, L.; Yang, W.; Yip, H.-L.; Huang, F.; Cao, Y. Wide bandgap dithienobenzodithiophene-based π-conjugated polymers consisting of fluorinated benzotriazole and benzothiadiazole for polymer solar cells. *J. Mater. Chem. C* **2016**, *4*, 4719–4727. [CrossRef]
57. Guo, P.; Luo, G.; Su, Q.; Li, J.; Zhang, P.; Tong, J.; Yang, C.; Xia, Y.; Wu, H. Boosting up performance of inverted photovoltaic cells from bis(alkylthien-2-yl)dithieno[2,3-*d*:2′,3′-*d*′]benzo[1,2-*b*:4′,5′-*b*′]dithiophene-based copolymers by advantageous vertical phase separation. *ACS Appl. Mater. Interfaces* **2017**, *9*, 10937–10945. [CrossRef]
58. Gao, P.; Tong, J.; Guo, P.; Li, J.; Wang, N.; Li, C.; Ma, X.; Zhang, P.; Wang, C.; Xia, Y. Medium band gap conjugated polymers from thienoacene derivatives and pentacyclic aromatic lactam as promising alternatives of poly(3-hexylthiophene) in photovoltaic application. *J. Polym. Sci. Part A Polym. Chem.* **2018**, *56*, 85–95. [CrossRef]

59. Shi, Q.; Fan, H.; Liu, Y.; Hu, W.; Li, Y.; Zhan, X. A copolymer of benzodithiophene with TIPS side chains for enhanced photovoltaic performance. *Macromolecules* **2011**, *44*, 9173–9179. [CrossRef]
60. Bathula, C.; Song, C.E.; Badgujar, S.; Hong, S.-J.; Kang, I.-N.; Moon, S.-J.; Lee, J.; Cho, S.; Shim, H.-K.; Lee, S.K. New TIPS-substituted benzo[1,2-*b*:4,5-*b*′]dithiophene-based copolymers for application in polymer solar cells. *J. Mater. Chem.* **2012**, *22*, 22224–22232. [CrossRef]
61. Kim, J.-H.; Song, C.E.; Shin, N.; Kang, H.; Wood, S.; Kang, I.-N.; Kim, B.J.; Kim, B.S.; Kim, J.-S.; Shin, W.S.; et al. High-crystalline medium-band-gap polymers consisting of benzodithiophene and benzotriazole derivatives for organic photovoltaic cells. *ACS Appl. Mater. Interfaces* **2013**, *5*, 12820–12831. [CrossRef]
62. Kim, J.-H.; Lee, M.; Yang, H.; Hwang, D.-H. A high molecular weight triisopropylsilylethynyl (TIPS)-benzodithiophene and diketopyrrolopyrrole-based copolymer for high performance organic photovoltaic cells. *J. Mater. Chem. A* **2014**, *2*, 6348–6352. [CrossRef]
63. Wang, L.; Liu, H.; Huai, Z.; Yang, S. Wide band gap and highly conjugated copolymers incorporating 2-(triisopropylsilylethynyl)thiophene-substituted benzodithiophene for efficient non-fullerene organic solar cells. *ACS Appl. Mater. Interfaces* **2017**, *9*, 28828–28837. [CrossRef] [PubMed]
64. Huang, F.; Wu, H.; Wang, D.; Yang, W.; Cao, Y. Novel electroluminescent conjugated polyelectrolytes based on polyfluorene. *Chem. Mater.* **2014**, *16*, 708–716. [CrossRef]
65. Tong, J.; An, L.; Li, J.; Lv, J.; Guo, P.; Li, L.; Zhang, P.; Yang, C.; Xia, Y.; Wang, C. Effects of alkyl side chain length of low bandgap naphtho[1,2-*c*:5,6-*c*′]bis[1,2,5]thiadiazole-based copolymers on the optoelectronic properties of polymer solar cells. *J. Polym. Sci. Part A Polym. Chem.* **2018**, *56*, 2059–2071. [CrossRef]
66. Guo, X.; Zhou, N.; Lou, S.J.; Smith, J.; Tice, D.B.; Hennek, J.W.; Ortiz, R.P.; Navarrete, J.T.L.; Li, S.; Strzalka, J.; et al. Polymer solar cells with enhanced fill factors. *Nat. Photonics* **2015**, *7*, 825–833. [CrossRef]
67. Carsten, B.; He, F.; Son, H.J.; Xu, T.; Yu, L. Stille polycondensation for synthesis of functional materials. *Chem. Rev.* **2011**, *111*, 1493–1528. [CrossRef]
68. Zhu, E.; Luo, G.; Liu, Y.; Yu, J.; Zhang, F.; Che, G.; Wu, H.; Tang, W. Triisopropylsilylethynyl substituted benzodithiophene copolymers: Synthesis, properties and photovoltaic characterization. *J. Mater. Chem. C* **2015**, *3*, 1595–1603. [CrossRef]
69. Murugesan, V.; de Bettignies, R.; Mercier, R.; Guillerez, S.; Perrin, L. Synthesis and characterizations of benzotriazole based donor-acceptor copolymers for organic photovoltaic applications. *Synth. Met.* **2012**, *162*, 1037–1045. [CrossRef]
70. Han, L.; Hu, T.; Bao, X.; Qiu, M.; Shen, W.; Sun, M.; Chen, W.; Yang, R. Steric minimization towards high planarity and molecular weight for aggregation and photovoltaic studies. *J. Mater. Chem. A* **2015**, *3*, 23587–23596. [CrossRef]
71. Li, G.; Zhao, B.; Kang, C.; Lu, Z.; Li, C.; Dong, H.; Hu, W.; Wu, H.; Bo, Z. Side chain influence on the morphology and photovoltaic performance of 5-fluoro-6-alkyloxybenzothiadiazole and benzodithiophene based conjugated polymers. *ACS Appl. Mater. Interfaces* **2015**, *7*, 10710–10717. [CrossRef]
72. Pommerehne, J.; Vestweber, H.; Guss, W.; Mahrt, R.F.; Bässler, H.; Porsch, M.; Daub, J. Efficient two layer leds on a polymer blend basis. *Adv. Mater.* **1995**, *7*, 551–554. [CrossRef]
73. Wu, P.-T.; Kim, F.S.; Champion, R.D.; Jenekhe, S.A. Conjugated Donor-Acceptor copolymer semiconductors. Synthesis, optical properties, electrochemistry, and field-effect carrier mobility of pyridopyrazine-based copolymers. *Macromolecules* **2008**, *41*, 7021–7028. [CrossRef]
74. Frisch, M.J.; Trucks, G.W.; Schlegel, H.B.; Scuseria, G.E.; Robb, M.A.; Cheeseman, J.R.; Scalmani, G.; Barone, V.; Mennucci, B.; Petersson, G.A.; et al. *Gaussian 09*; Revision A. 01; Gaussian, Inc.: Wallingford, CT, USA, 2009.
75. He, Z.; Zhong, C.; Su, S.; Xu, M.; Wu, H.; Cao, Y. Enhanced power-conversion efficiency in polymer solar cells using an inverted device structure. *Nat. Photonics* **2012**, *6*, 591–595. [CrossRef]
76. Bai, Y.; Yang, B.; Zhao, C.; Shi, Z.; Hayat, T.; Alsaedi, A.; Tan, Z. Synergy of a titanium chelate electron collection layer and a vertical phase separated photoactive layer for efficient inverted polymer solar cells. *J. Mater. Chem. A* **2018**, *6*, 7257–7264. [CrossRef]
77. Blom, P.W.M.; Mihailetchi, V.D.; Koster, L.J.A.; Markov, D.E. Device physics of polymer: Fullerene bulk heterojunction solar cells. *Adv. Mater.* **2007**, *19*, 1551–1566. [CrossRef]
78. He, Z.; Xiao, B.; Liu, F.; Wu, H.; Yang, Y.; Xiao, S.; Wang, C.; Russell, T.P.; Cao, Y. Single-junction polymer solar cells with high efficiency and photovoltage. *Nat. Photonics* **2015**, *9*, 174–179. [CrossRef]

79. Güldal, N.S.; Berlinghof, M.; Kassar, T.; Du, X.; Jiao, X.; Meyer, M.; Ameri, T.; Osvet, A.; Li, N.; Destri, G.L.; et al. Controlling additive behavior to reveal an alternative morphology formation mechanism in polymer:fullerene bulk-heterojunctions. *J. Mater. Chem. A* **2016**, *4*, 16136–16147. [CrossRef]
80. Lee, J.K.; Ma, W.L.; Brabec, C.J.; Yuen, J.; Moon, J.S.; Kim, J.Y.; Lee, K.; Bazan, G.C.; Heeger, A.J. Processing additives for improved efficiency from bulk heterojunction solar cells. *J. Am. Chem. Soc.* **2018**, *130*, 3619–3623. [CrossRef]
81. Wienk, M.M.; Kroon, J.M.; Verhees, W.J.H.; Knol, J.; Hummelen, J.C.; van Hal, P.A.; Janssen, R.A.J. Efficient methano[70]fullerene/MDMO-PPV bulk heterojunction photovoltaic cells. *Angew. Chem.* **2003**, *115*, 3493–3497. [CrossRef]
82. Li, J.; Liang, Z.; Wang, Y.; Li, H.; Tong, J.; Bao, X.; Xia, Y. Enhanced efficiency of polymer solar cells through synergistic optimization of mobility and tuning donor alloys by adding high-mobility conjugated polymers. *J. Mater. Chem. C* **2018**, *6*, 11015–11022. [CrossRef]
83. Kim, T.; Lee, J.Y.; Heo, J.; Lim, B.; Kim, J.Y. Highly efficient polymer solar cells with a thieno-pyrroledione and benzodithiophene containing planar random copolymer. *Polym. Chem.* **2018**, *9*, 1216–1222. [CrossRef]